Supporting Information for "The Sensitivity of Surface Mass Loading Displacement Response to Perturbations in the Elastic Structure of the Crust and Mantle"

Hilary R. Martens,[1] Luis Rivera,[2] Mark Simons,[1] and Takeo Ito[3]

Contents of this file

1. Figures S1 to S26

Additional Supporting Information (Files uploaded separately)

1. Captions for Datasets S1 to S24

Introduction

This supporting information provides tables of the seismic velocity and density profiles for each of the six reference Earth models used in our study. We also provide tables of load Love numbers (LLNs) and load Green's functions (LGFs), in both the CE and CM reference frames, derived directly from each of the reference Earth models. Methods for computing the LLNs and LGFs are described in the main text and implemented using our internally developed software package, `LoadDef`.

In the main text, we present partial derivatives of LLNs for spherical harmonic degrees 2, 100, and 10000, derived from the reference Earth model PREM (Figs. 1–3). Figure S1 shows the partial derivatives of the LLNs for a homogeneous sphere. Figures S2–S4 show partial derivatives for $n = 2$ derived from Earth model 1066A, which may be compared directly with *Okubo and Saito* [1983]. In addition, we show partial derivatives of load, potential, shear, and stress Love numbers derived from PREM for a selection of other spherical harmonic degrees in Figs. S5–S17.

Figure S18 depicts displacement LGFs for a homogeneous sphere model. Figure S19 shows a zoomed-in version of Fig. 6 from the main text. Figure S20 depicts LGF sensitivity kernels for perturbations to layers of 50-km thickness through the crust and upper mantle (cf. Fig. 7 from the main text). Figures S21 and S22 are identical to Figs. 15 and 16 in the main text, respectively, albeit for the second profile line (B–B′) from Fig. 11 in the main text. Figures S23–S25 show the global spatial distributions of the east, north, and vertical components of the vector differences between pairs of predicted M_2 OTL-induced surface displacements derived from PREM and STW105. The vector differences for additional forward-model combinations are shown as histograms in Figure S26.

Table S1 provides a list of degree-2 potential Love numbers for six seismologically derived Earth models.

Data Set S1. Radial profiles of density (ρ), P-wave velocity (V_P), and S-wave velocity (V_S) for the isotropic and oceanless version of the Preliminary Reference Earth Model (PREM) used in our study. We generated the model using the polynomial functions from Table 1 of *Dziewonski and Anderson* [1981], evaluated every 100 km within the core regions and every 100 m within the mantle and crust. We also assumed effective isotropic velocities between 220 and 24.4 km depth and replaced the water layer at the surface by the properties of the upper-most crust: $V_P = 5800$ m s^{-1}, $V_S = 3200$ m s^{-1}, and $\rho = 2600$ kg m^{-3}.

Data Set S2. Radial profiles of ρ, V_P, and V_S for STW105 [*Kustowski et al.*, 2008]. We acquired the model directly from the Incorporated Research Institutions for Seismology (IRIS) Data Management Center (DMC) [*Trabant et al.*, 2012] and replaced the water layer at the surface with typical values for the upper crust.

Data Set S3. Radial profiles of ρ, V_P, and V_S for AK135f. AK135f was derived from seismic body waves [*Kennett et al.*, 1995], with density and Q structure contributed by *Montagner and Kennett* [1996]. We acquired the model directly from the IRIS DMC and replaced the water layer at the surface with typical values for the upper crust.

Data Set S4. Radial profiles of ρ, V_P, and V_S for the Earth model 1066A, which we acquired from Table 5 of *Gilbert and Dziewonski* [1975].

Data Set S5. Radial profiles of ρ, V_P, and V_S for the Earth model SNA, derived from an average of upper mantle shear-wave velocity structure in North America [*Grand and Helmberger*, 1984]. Below 1000 km depth, the model assumes the structural properties of AK135f.

Data Set S6. Radial profiles of ρ, V_P, and V_S for the Earth model CR, derived from an average of upper mantle P-wave velocity structure beneath stable North America [*Chu et al.*, 2012]. The values for V_S and ρ were obtained from ratios of AK135 (Risheng Chu, personal communication). Below 1000 km depth, the model assumes the structural properties of AK135f.

Data Set S7. Load Love numbers (h'_n, l'_n and k'_n) derived from PREM (Data Set S1) up to spherical harmonic degree 10000. Asymptotic values for the Love numbers, computed using the second-order expressions derived by *Guo et al.* [2004], are provided in the final three columns.

Data Set S8. Same as Data Set S7, but the load Love numbers are instead derived from STW105 (Data Set S2).

Data Set S9. Same as Data Set S7, but the load Love numbers are instead derived from AK135f (Data Set S3).

Data Set S10. Same as Data Set S7, but the load Love numbers are instead derived from 1066A (Data Set S4).

Data Set S11. Same as Data Set S7, but the load Love numbers are instead derived from SNA (Data Set S5).

Data Set S12. Same as Data Set S7, but the load Love numbers are instead derived from CR (Data Set S6).

Data Set S13. Load Green's functions in the CE reference frame derived from PREM (Data Set S1). The first column lists the angular distance between an observer and the load point in degrees, the second column provides the vertical-component of the elastic displacement response in meters per kilogram, and the third column provides the horizontal-component of the elastic displacement response in meters per kilogram. The fourth and fifth columns represent the second and third columns, respectively, multiplied by a factor of $10^{12}a\theta$, where a is Earth's radius in meters and θ is the observer-to-load angular distance in radians.

[1]Seismological Laboratory, Division of Geological and Planetary Sciences, California Institute of Technology, Pasadena, California, USA.

[2]Institut de Physique du Globe de Strasbourg (UMR7516), Université de Strasbourg/CNRS, Strasbourg, France.

[3]Graduate School of Environmental Studies, Nagoya University, Nagoya, Japan.

0148-0227/16/$9.00

Data Set S14. Same as Data Set 13, but for load Green's functions derived from STW105 (Data Set S2).
Data Set S15. Same as Data Set 13, but for load Green's functions derived from AK135f (Data Set S3).
Data Set S16. Same as Data Set 13, but for load Green's functions derived from 1066A (Data Set S4).
Data Set S17. Same as Data Set 13, but for load Green's functions derived from SNA (Data Set S5).
Data Set S18. Same as Data Set 13, but for load Green's functions derived from CR (Data Set S6).
Data Set S19. Same as Data Set 13, but for the CM reference frame.
Data Set S20. Same as Data Set 14, but for the CM reference frame.
Data Set S21. Same as Data Set 15, but for the CM reference frame.
Data Set S22. Same as Data Set 16, but for the CM reference frame.
Data Set S23. Same as Data Set 17, but for the CM reference frame.
Data Set S24. Same as Data Set 18, but for the CM reference frame.

References

Chu, R., B. Schmandt, and D. V. Helmberger (2012), Upper mantle P velocity structure beneath the Midwestern United States derived from triplicated waveforms, *Geochemistry, Geophysics, Geosystems*, *13*(2), doi:10.1029/2011GC003818.

Dziewonski, A. M., and D. L. Anderson (1981), Preliminary reference Earth model, *Physics of the earth and planetary interiors*, *25*(4), 297–356, doi:10.1016/0031-9201(81)90046-7.

Gilbert, F., and A. Dziewonski (1975), An application of normal mode theory to the retrieval of structural parameters and source mechanisms from seismic spectra, *Philosophical Transactions of the Royal Society of London. Series A, Mathematical and Physical Sciences*, *278*(1280), 187–269.

Grand, S. P., and D. V. Helmberger (1984), Upper mantle shear structure of North America, *Geophysical Journal International*, *76*(2), 399–438, doi:10.1111/j.1365-246X.1984.tb05053.x.

Guo, J., Y. Li, Y. Huang, H. Deng, S. Xu, and J. Ning (2004), Green's function of the deformation of the Earth as a result of atmospheric loading, *Geophysical journal international*, *159*(1), 53–68, doi:10.1111/j.1365-246X.2004.02410.x.

Kennett, B., E. Engdahl, and R. Buland (1995), Constraints on seismic velocities in the Earth from traveltimes, *Geophysical Journal International*, *122*(1), 108–124, doi:10.1111/j.1365-246X.1995.tb03540.x.

Kustowski, B., G. Ekström, and A. Dziewoński (2008), Anisotropic shear-wave velocity structure of the Earth's mantle: A global model, *Journal of Geophysical Research: Solid Earth*, *113*(B06306), doi:10.1029/2007JB005169.

Montagner, J.-P., and B. Kennett (1996), How to reconcile body-wave and normal-mode reference Earth models, *Geophysical Journal International*, *125*(1), 229–248, doi:10.1111/j.1365-246X.1996.tb06548.x.

Okubo, S., and T. Endo (1986), Static spheroidal deformation of degree 1 - Consistency relation, stress solution and partials, *Geophysical Journal International*, *86*(1), 91–102, doi:10.1111/j.1365-246X.1986.tb01074.x.

Okubo, S., and M. Saito (1983), Partial derivative of Love numbers, *Bulletin géodésique*, *57*(1), 167–179.

Trabant, C., A. R. Hutko, M. Bahavar, R. Karstens, T. Ahern, and R. Aster (2012), Data products at the IRIS DMC: Stepping stones for research and other applications, *Seismological Research Letters*, *83*(5), 846–854, doi:10.1785/0220120032.

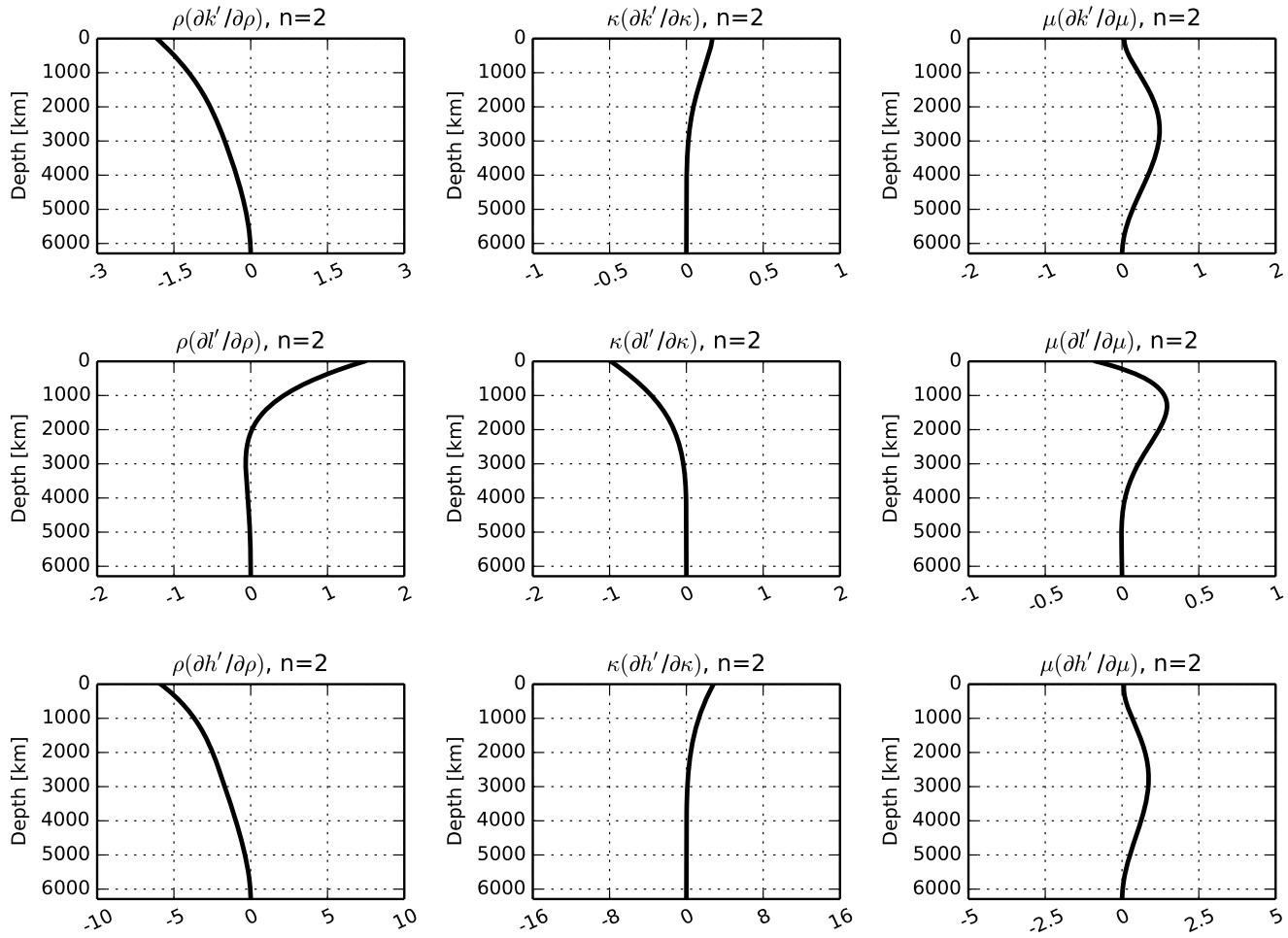

Figure S1. Partial derivatives of degree-2 load Love numbers with respect to the shear modulus, μ, the bulk modulus, κ, and density, ρ, for a homogeneous sphere model of properties $V_P = 10000$ m s^{-1}, $V_S = 5000$ m s^{-1}, and $\rho = 5000$ kg m^{-3}. The partial derivatives were computed using the techniques discussed by *Okubo and Saito* [1983]. Here, the profiles extend through the whole Earth, which is entirely solid. The partials have been multiplied by the depth profile of each elastic parameter, making them dimensionless. The horizontal axes are in units of 10^{-4} km^{-1}.

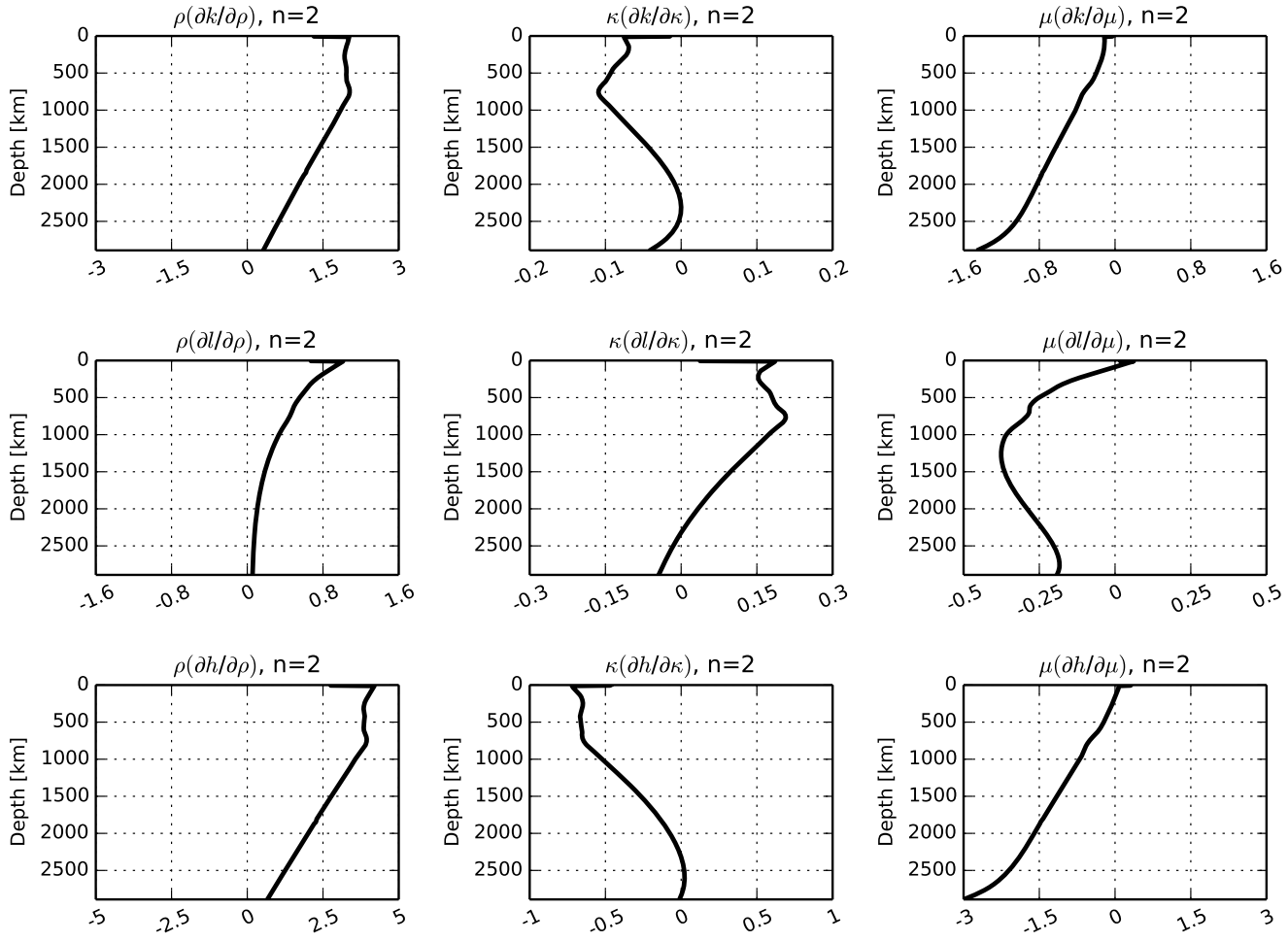

Figure S2. Partial derivatives of degree-2 potential Love numbers with respect to the shear modulus, μ, the bulk modulus, κ, and density, ρ, for Earth model 1066A [*Gilbert and Dziewonski*, 1975], computed using the techniques discussed by *Okubo and Saito* [1983]. The partials have been multiplied by the depth profile of each elastic parameter, making them dimensionless. The horizontal axes are in units of 10^{-4} km^{-1}. The figure may be compared directly with fig. 1a in *Okubo and Saito* [1983] for Earth's crust and mantle.

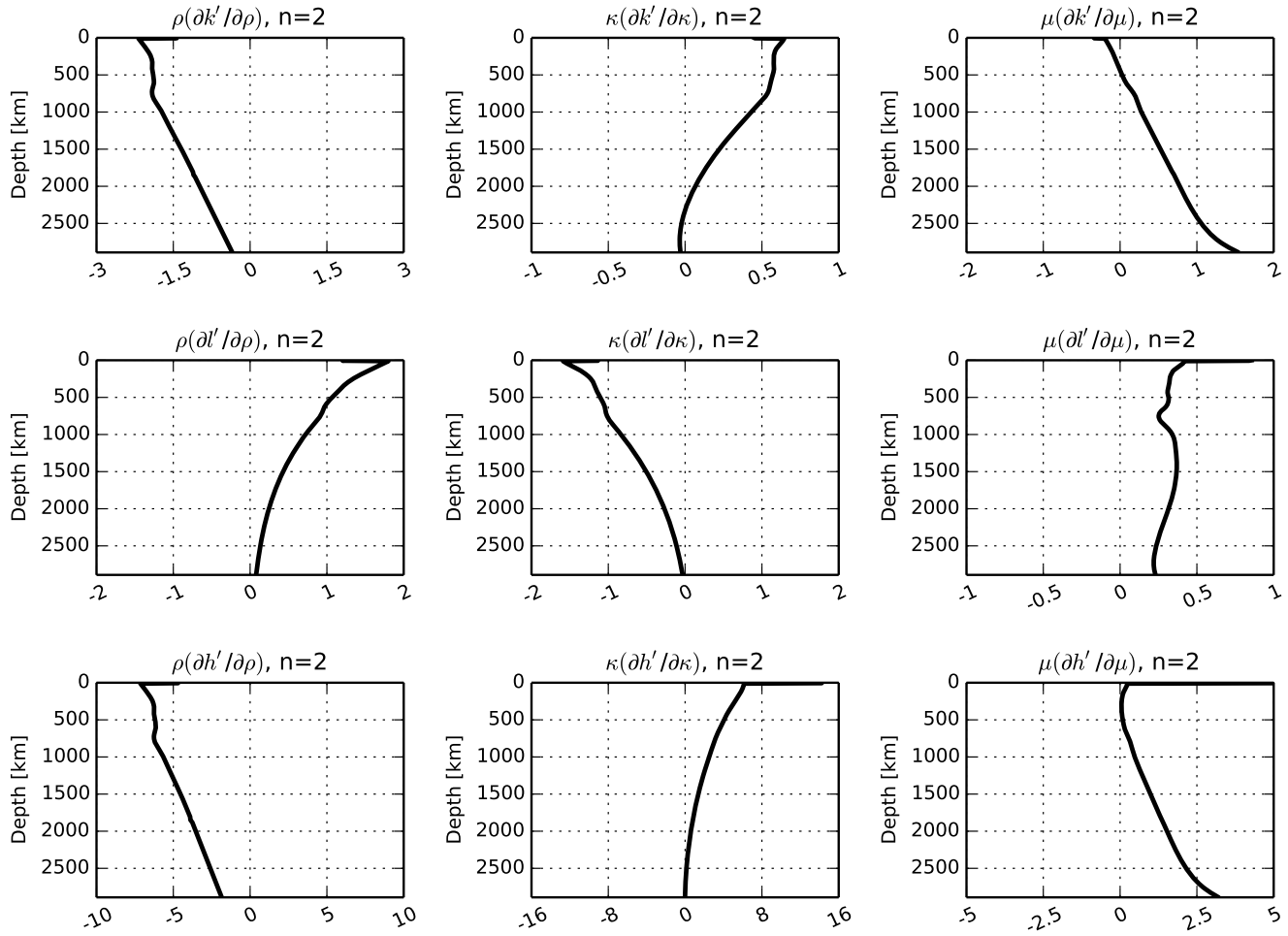

Figure S3. Same as Fig. S2, but for load, rather than potential, Love numbers (cf. *Okubo and Saito* [1983], fig. 1b). The horizontal axes are in units of 10^{-4} km^{-1}.

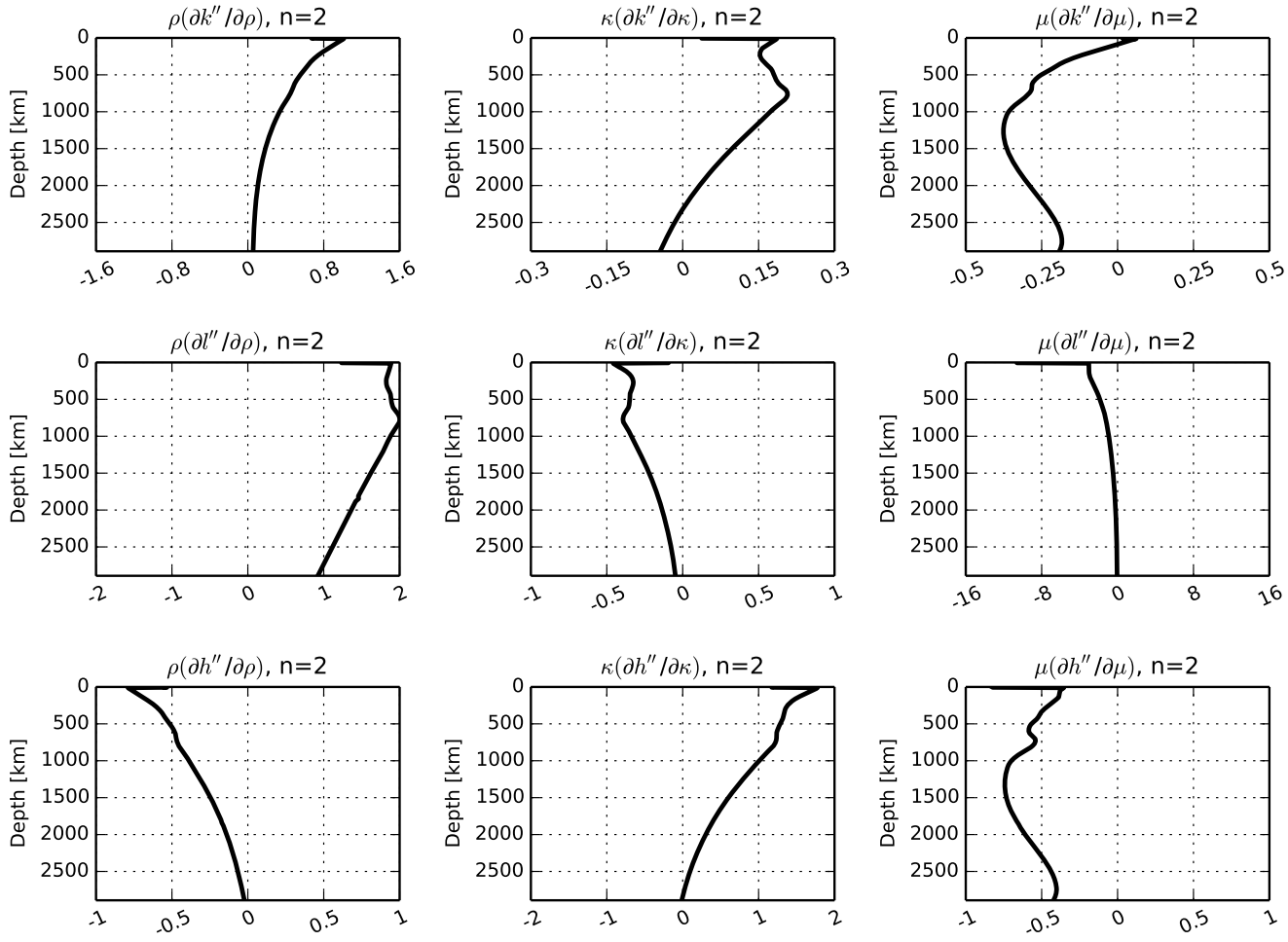

Figure S4. Same as Fig. S2, but for shear, rather than potential, Love numbers (cf. *Okubo and Saito* [1983], fig. 1c). The horizontal axes are in units of 10^{-4} km^{-1}.

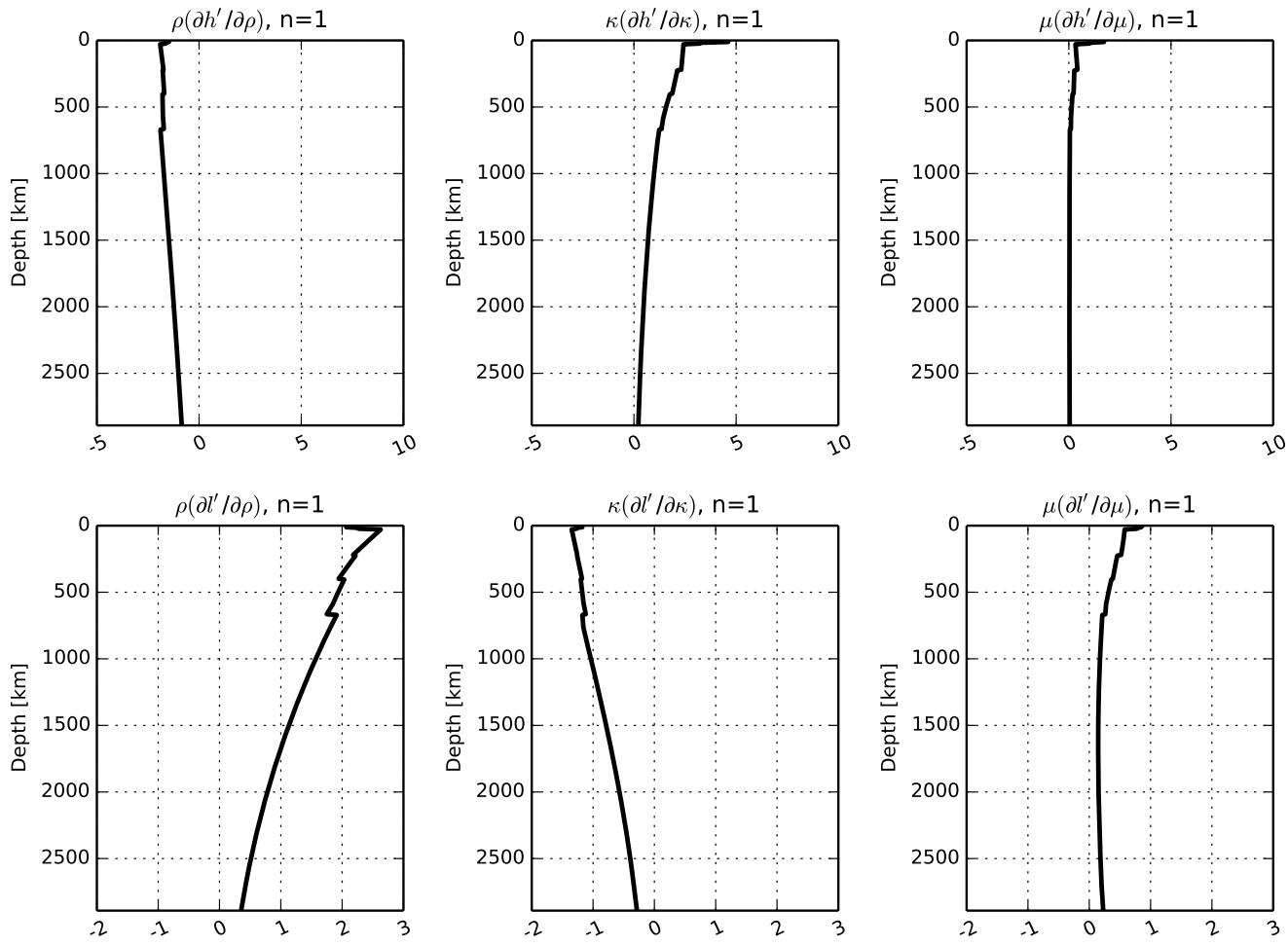

Figure S5. Partial derivatives of degree-1 load Love numbers with respect to the shear modulus, μ, the bulk modulus, κ, and density, ρ, for Earth model PREM, computed using the techniques discussed by *Okubo and Endo* [1986] and *Okubo and Saito* [1983]. The partials have been multiplied by the depth profile of each elastic parameter, making them dimensionless. The horizontal axes are in units of 10^{-4} km^{-1}.

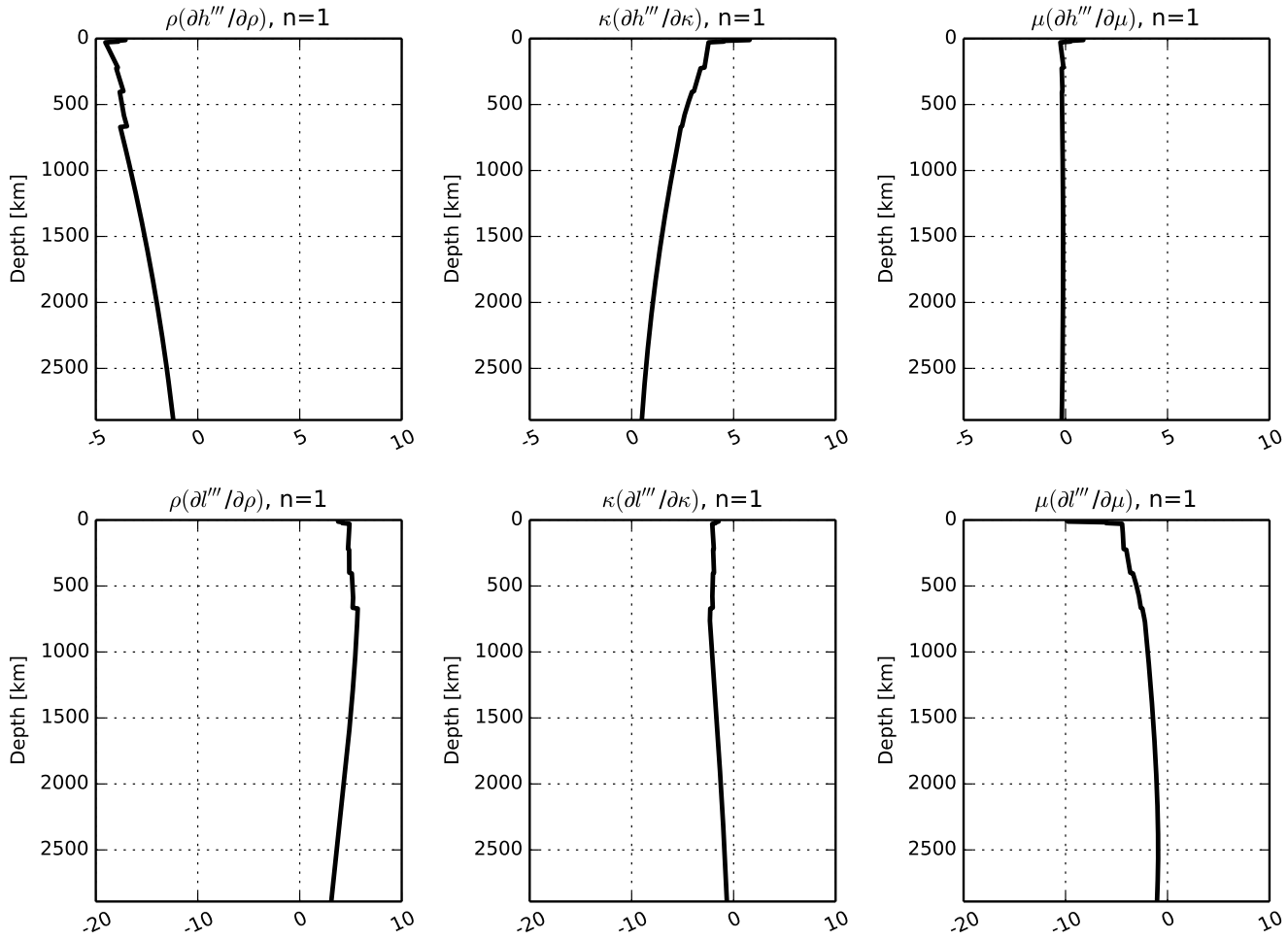

Figure S6. Same as Fig. S5, but for stress Love numbers (see Table 1 in the main text for the relevant surface boundary conditions). The horizontal axes are in units of 10^{-4} km^{-1}.

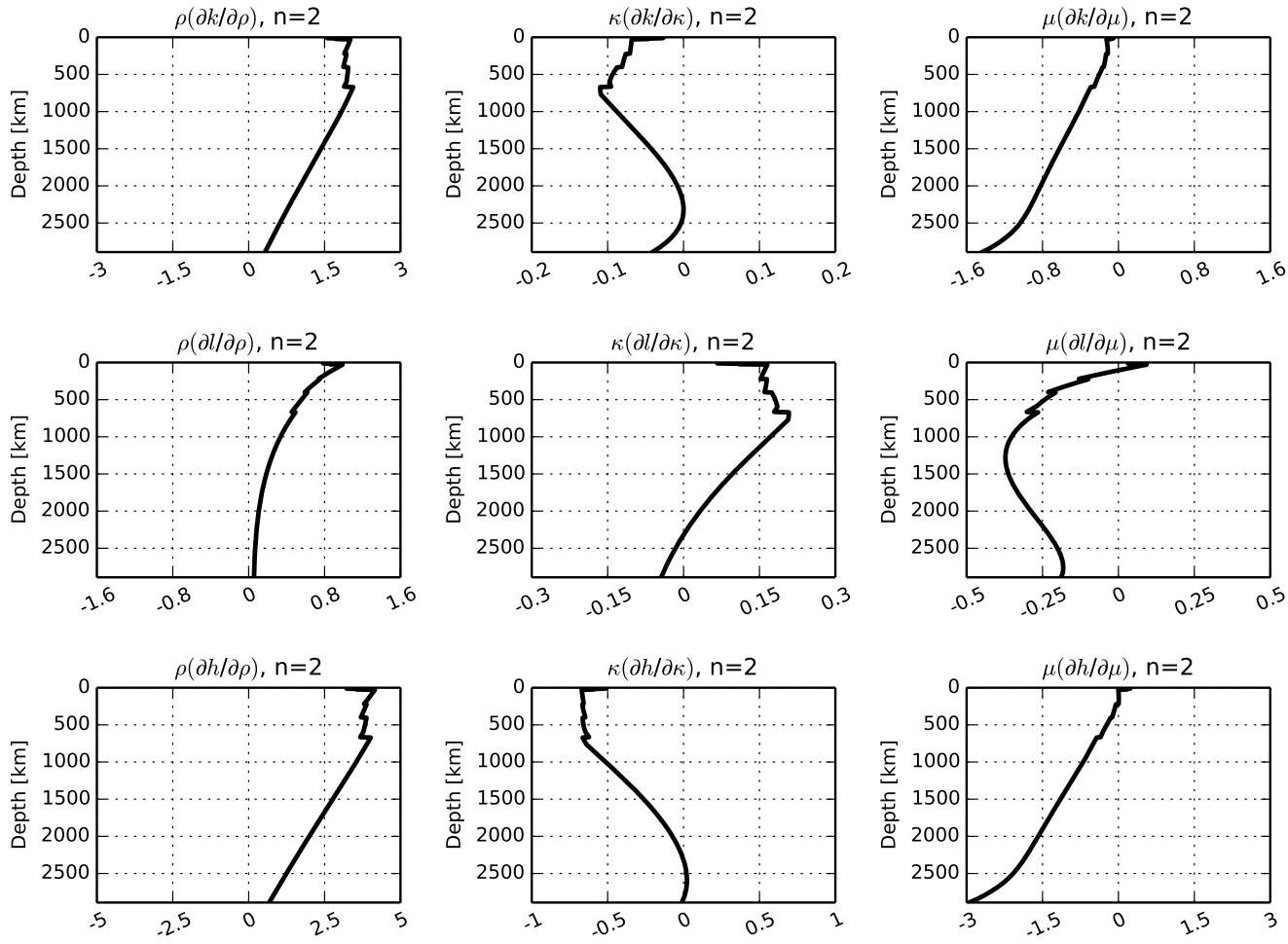

Figure S7. Partial derivatives of degree-2 potential Love numbers with respect to the shear modulus, μ, the bulk modulus, κ, and density, ρ, for Earth model PREM. The partials have been multiplied by the depth profile of each elastic parameter, making them dimensionless. The horizontal axes are in units of 10^{-4} km^{-1}. Note that this figure is identical to Fig. S2, but here the partials are computed based on PREM rather than 1066A.

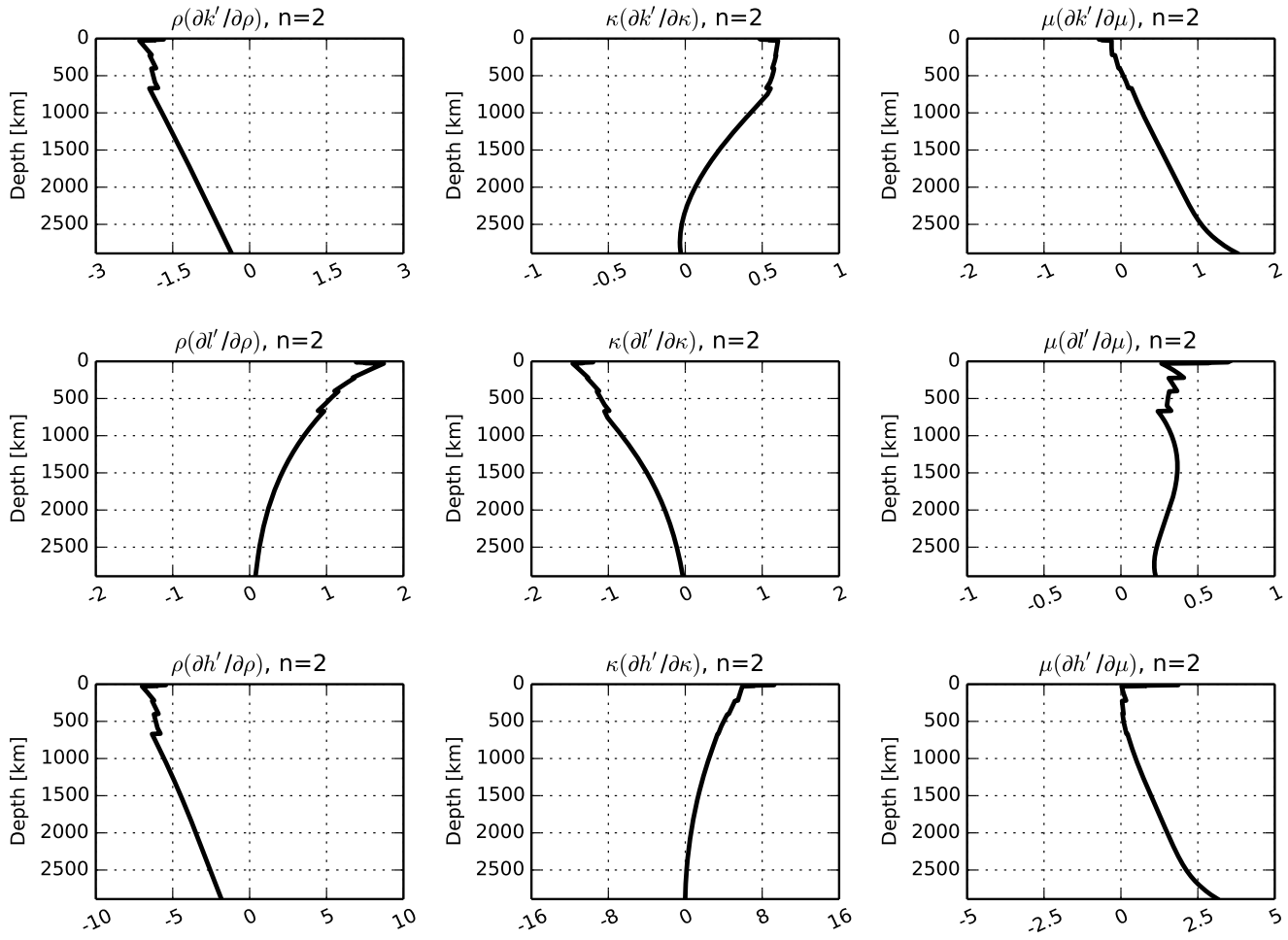

Figure S8. Same as Fig. S7, but for load Love numbers. Note that this figure is identical to Fig. S3, but here the partials are computed based on PREM rather than 1066A. The horizontal axes are in units of 10^{-4} km^{-1}.

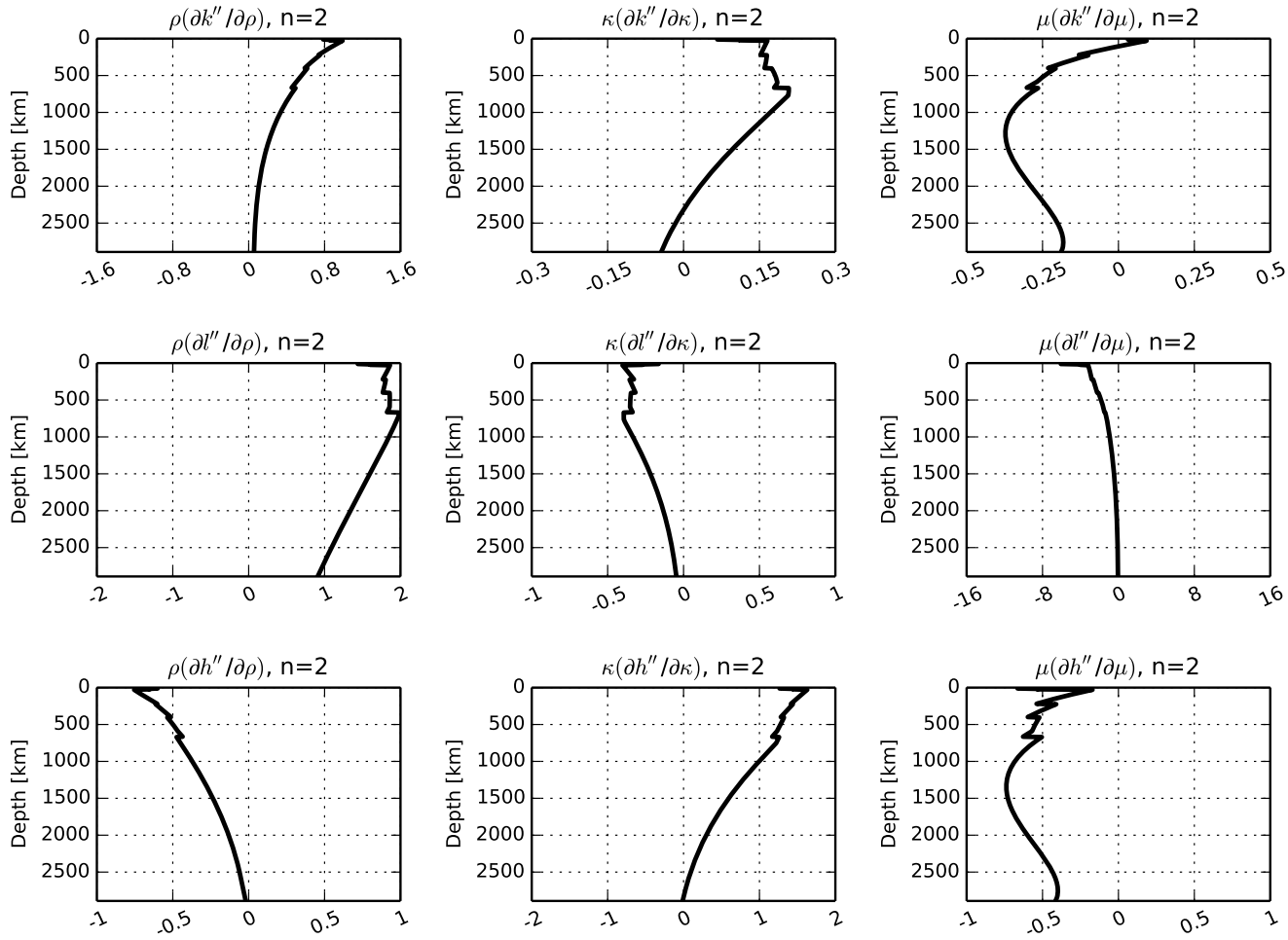

Figure S9. Same as Fig. S7, but for shear Love numbers. Note that this figure is identical to Fig. S4, but here the partials are computed based on PREM rather than 1066A. The horizontal axes are in units of 10^{-4} km^{-1}.

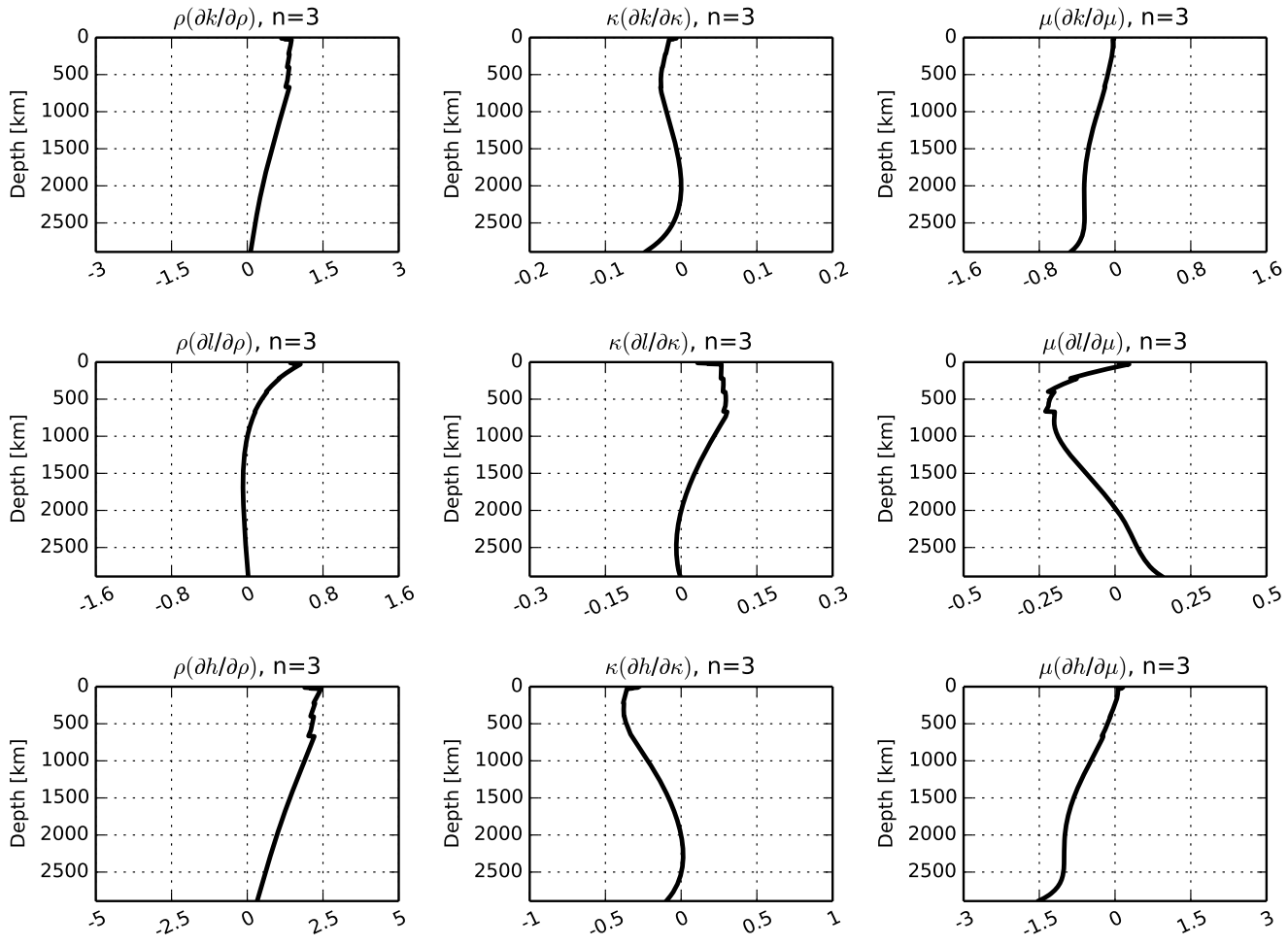

Figure S10. Same as Fig. S7, but for spherical harmonic degree $n = 3$.

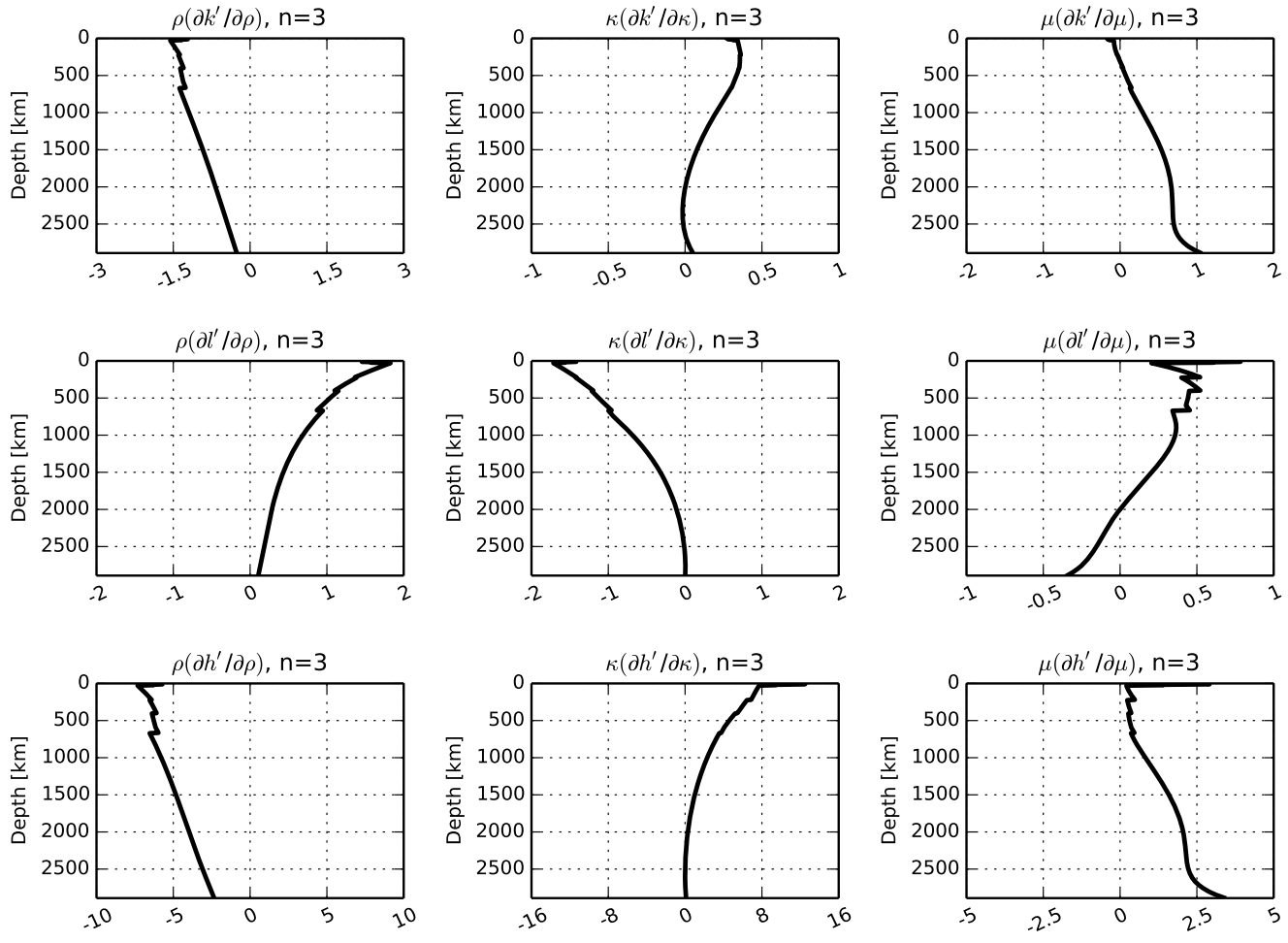

Figure S11. Same as Fig. S8, but for spherical harmonic degree $n = 3$.

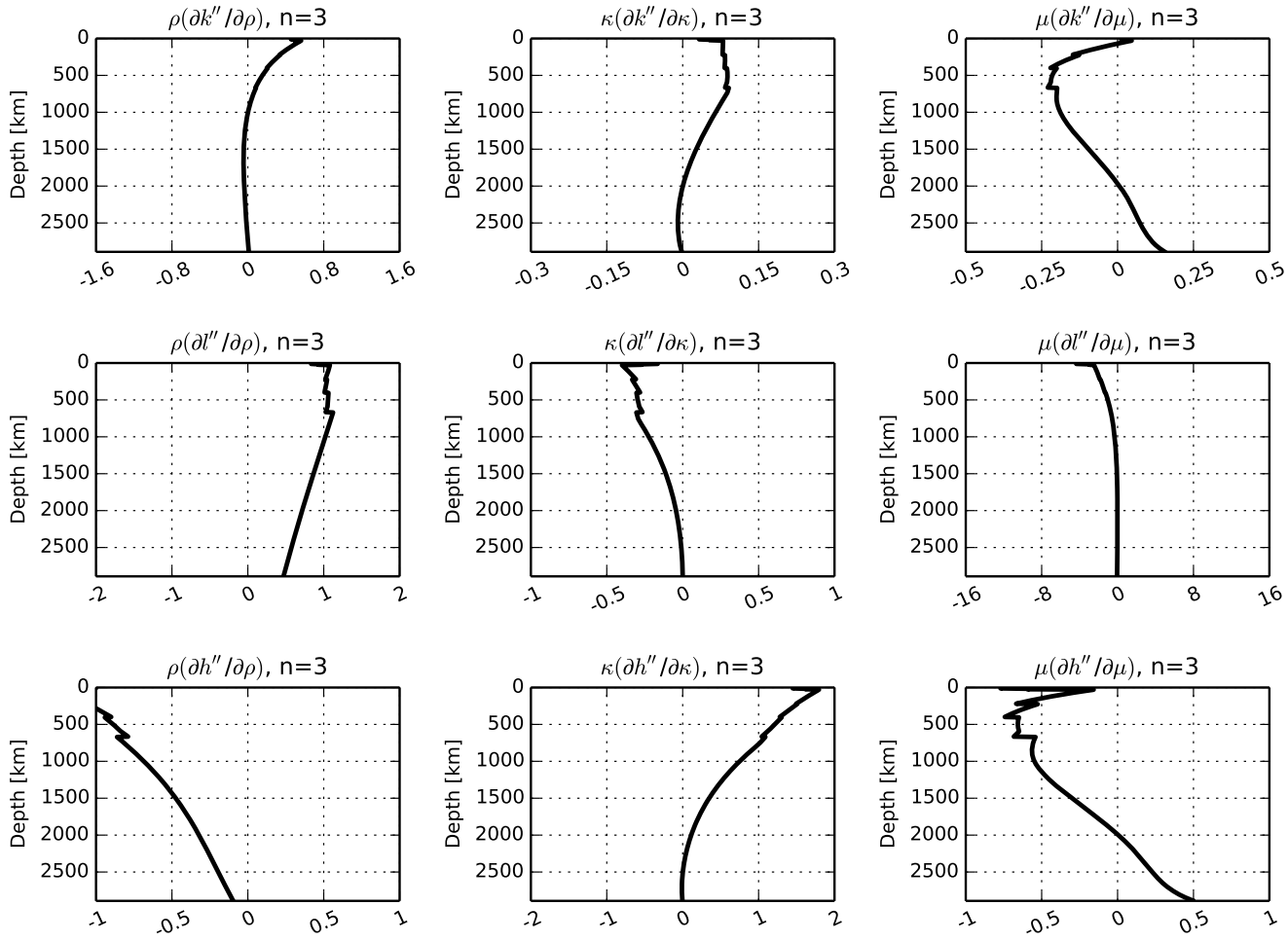

Figure S12. Same as Fig. S9, but for spherical harmonic degree $n = 3$.

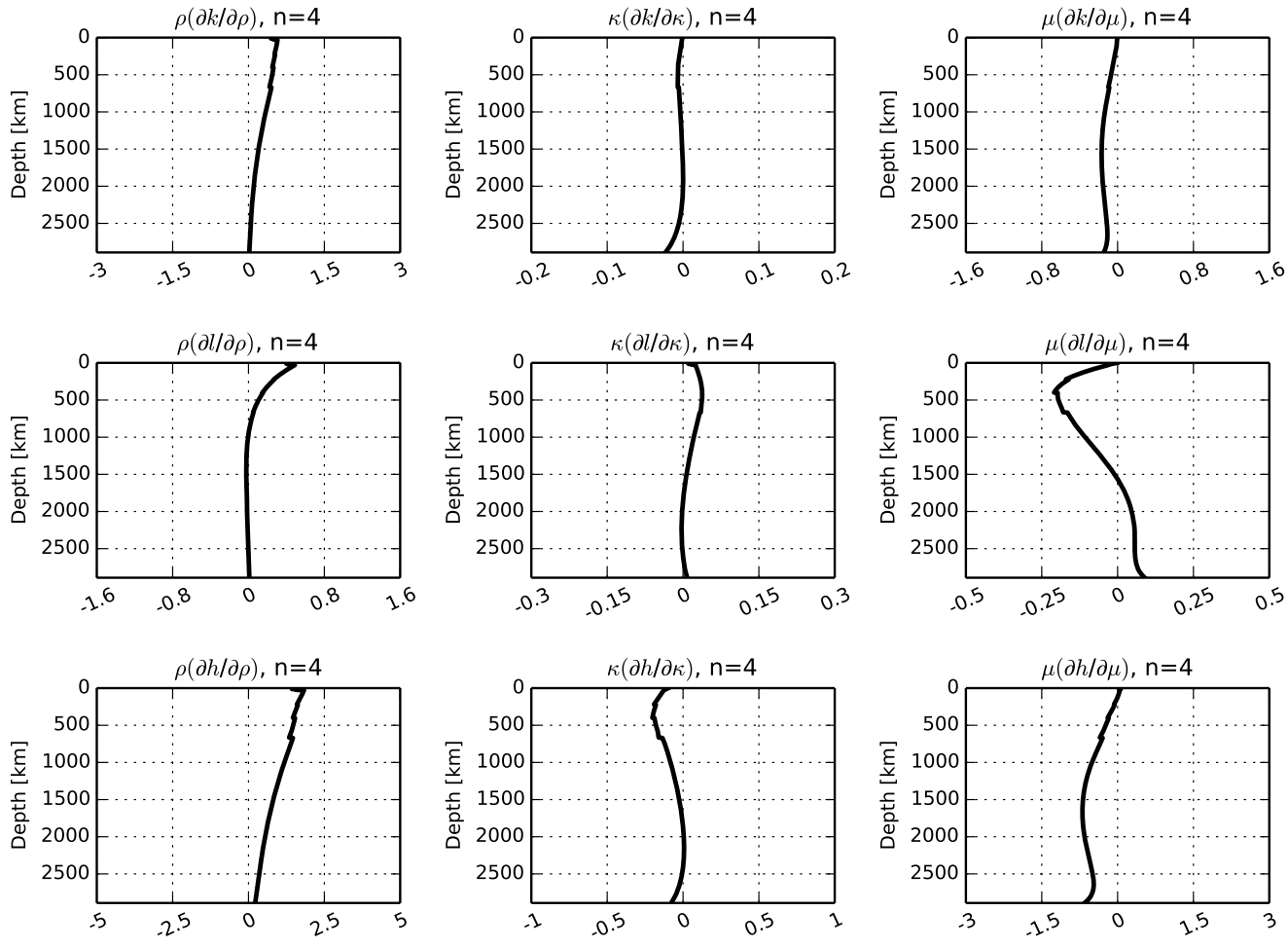

Figure S13. Same as Fig. S7, but for spherical harmonic degree $n = 4$.

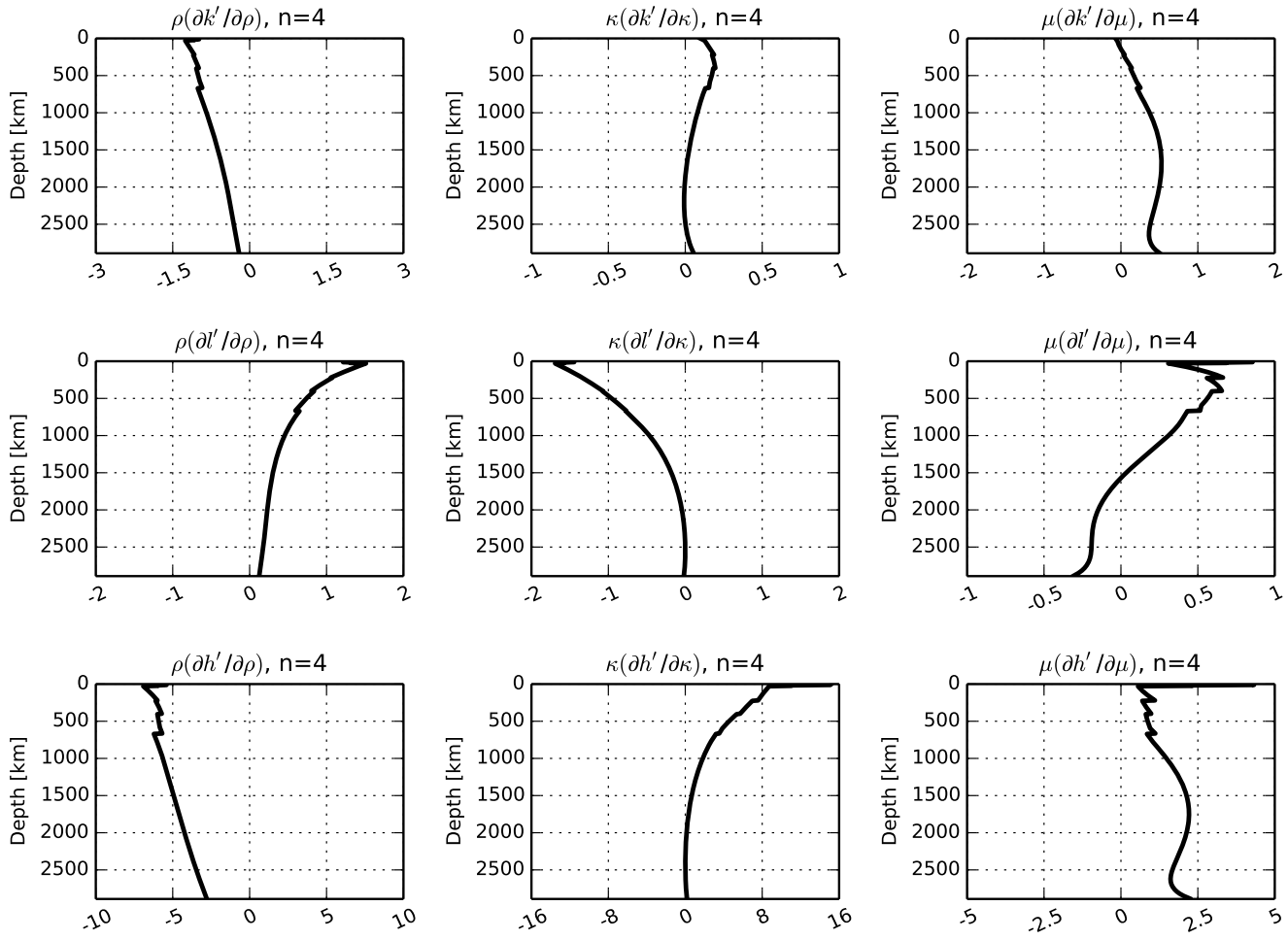

Figure S14. Same as Fig. S8, but for spherical harmonic degree $n = 4$.

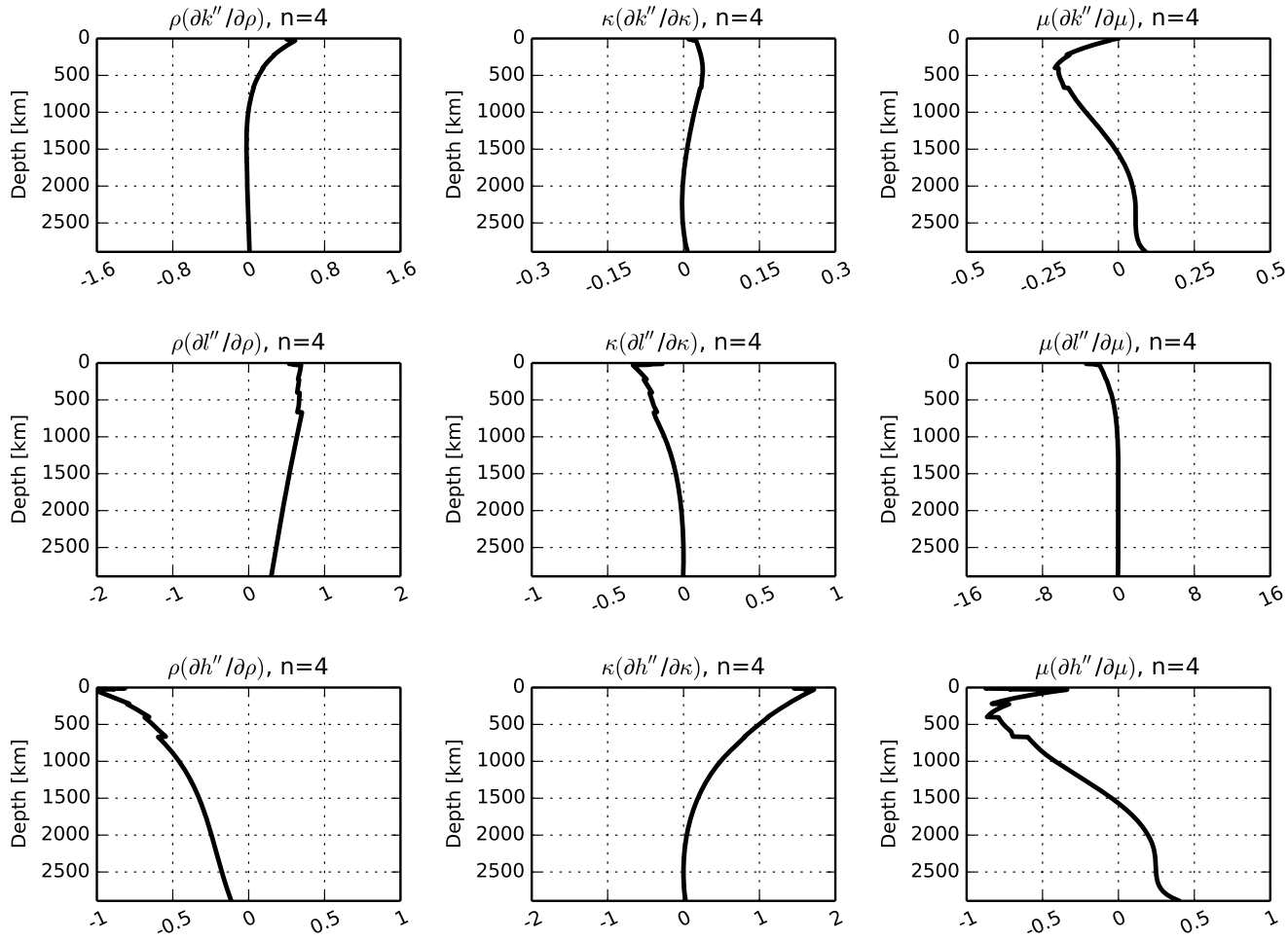

Figure S15. Same as Fig. S9, but for spherical harmonic degree $n = 4$.

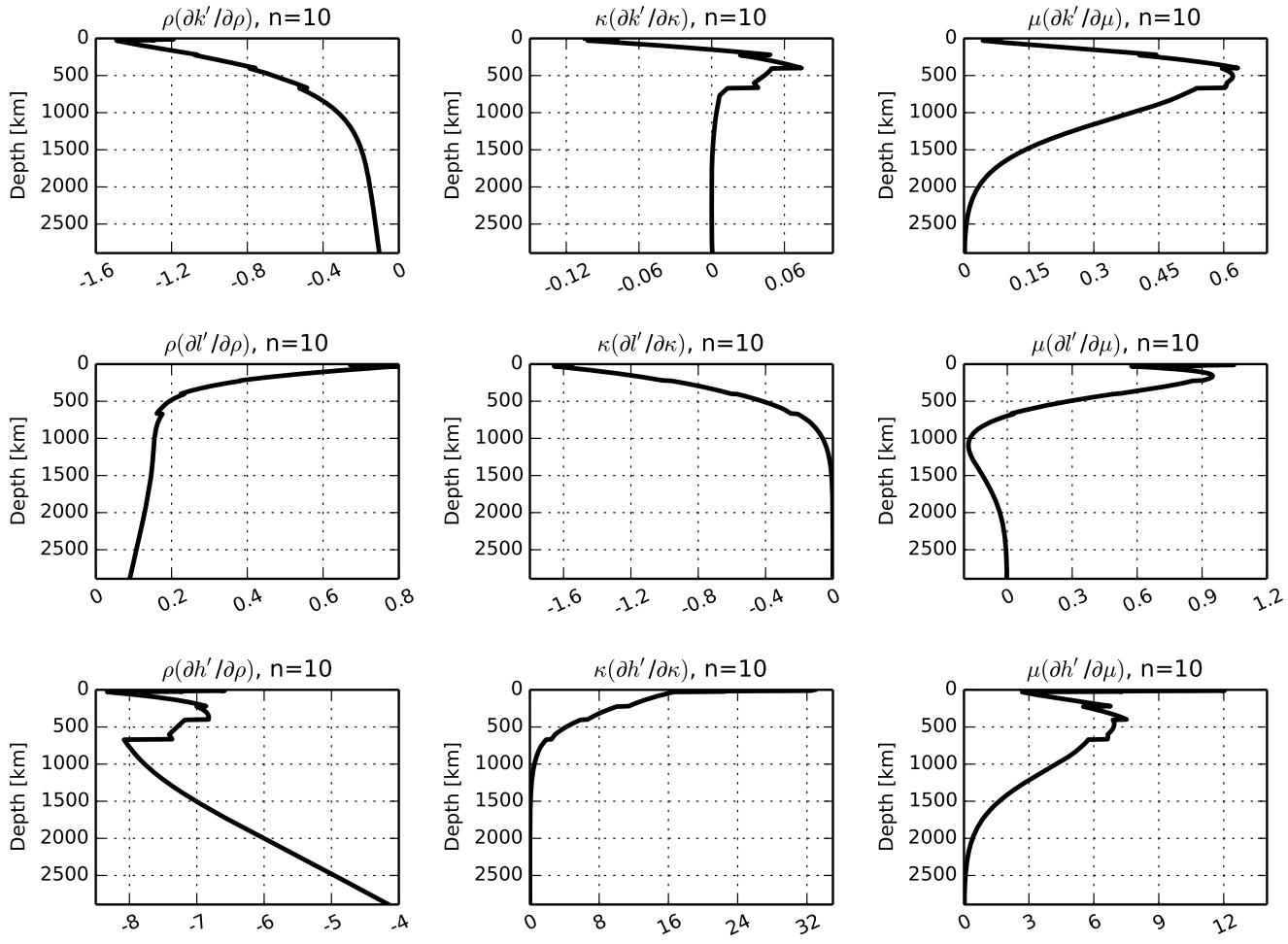

Figure S16. Same as Fig. S8, but for spherical harmonic degree $n = 10$.

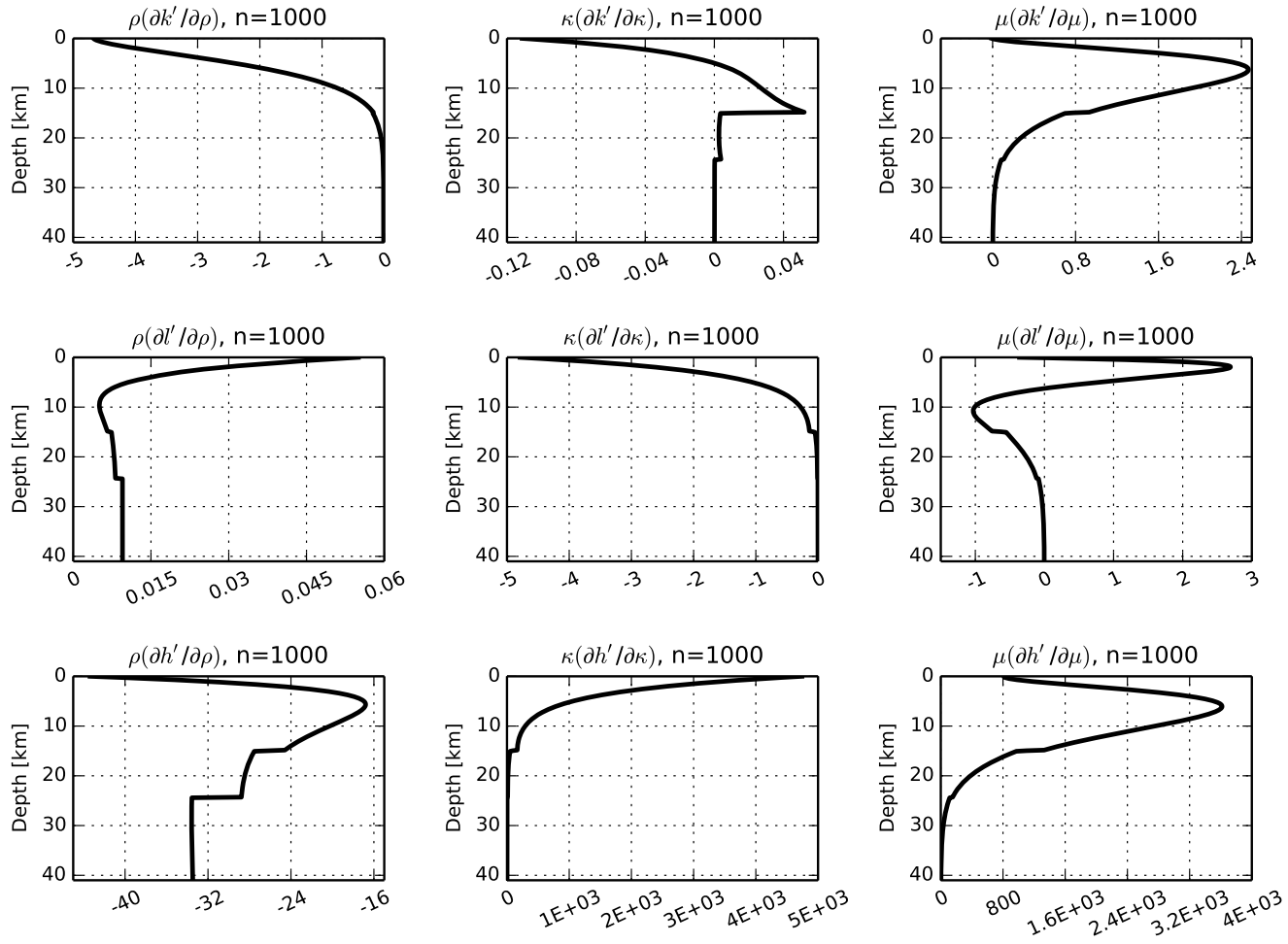

Figure S17. Same as Fig. S8, but for spherical harmonic degree $n = 1000$.

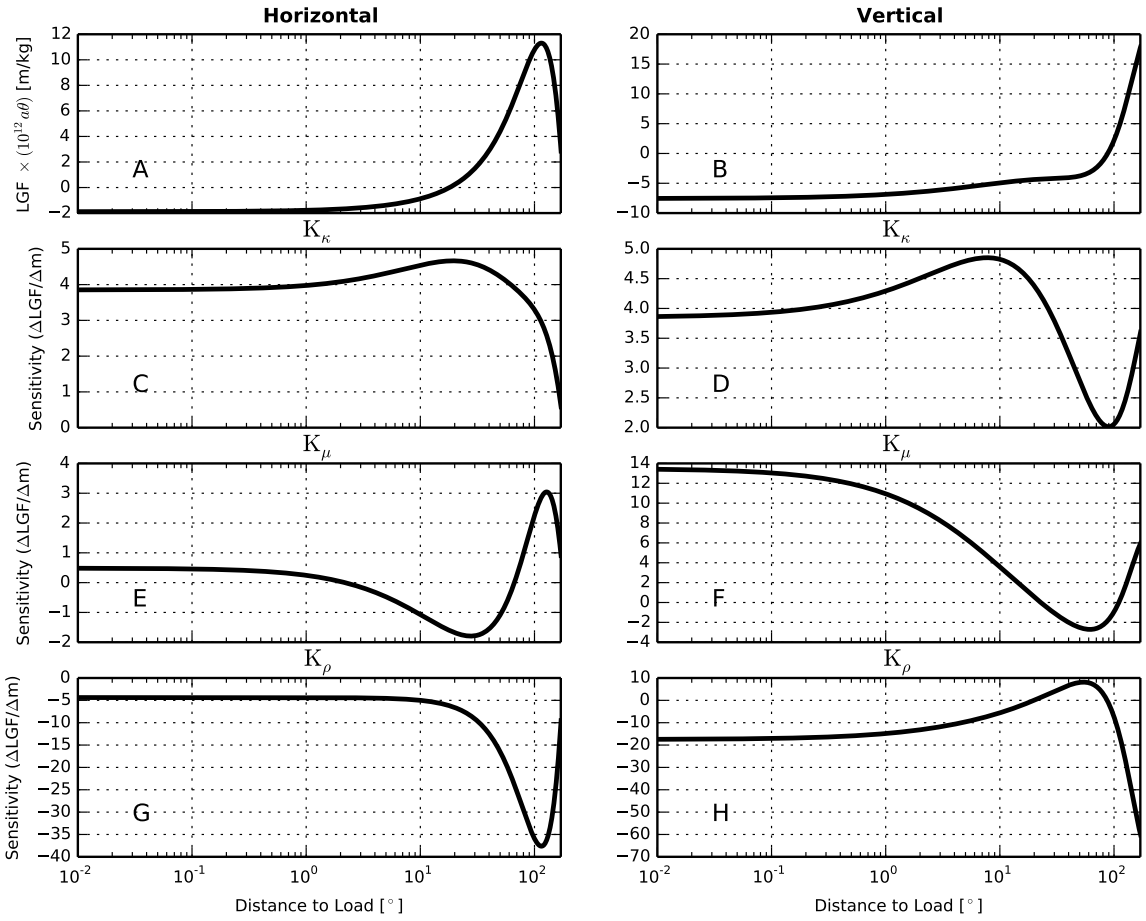

Figure S18. Displacement-response sensitivity kernels for 1% linear perturbations to the bulk modulus (κ), shear modulus (μ), and density (ρ) of a homogeneous sphere with properties $V_P = 10000$ m s^{-1}, $V_S = 5000$ m s^{-1}, and $\rho = 5000$ kg m^{-3}. Since the elastic properties (μ, κ and ρ) are Jeffrey's parameters, we define the model terms in common-log space. Explicitly, $\mathbf{m}_\mu = \log_{10}\mu$, $\mathbf{m}_\kappa = \log_{10}\kappa$ and $\mathbf{m}_\rho = \log_{10}\rho$. For a 1% linear perturbation to the elastic moduli and density, the model-parameter perturbation is $\Delta\mathbf{m}^j_\beta = \log_{10}(1.01)$. The horizontal components of the displacement LGFs and sensitivity kernels are shown in the left panels; the vertical components are shown in the right panels. The top panels (A & B) depict the displacement LGFs in the CM reference frame derived from the original, unperturbed model. The lower panels depict the LGF sensitivities resulting from perturbations to the κ (C & D), μ (E & F), and ρ (G & H) model parameters. Sensitivities are computed as the change in LGF per change in model parameter. The displacement LGFs, as well as the sensitivity kernels, were multiplied by the factor $10^{12}a\theta$ to remove the singularity at the load point and to normalize the magnitude of the response, where a is Earth's radius in meters and θ is the angular distance from the load point in radians. Units of the unnormalized LGFs are meters of displacement per kilogram load.

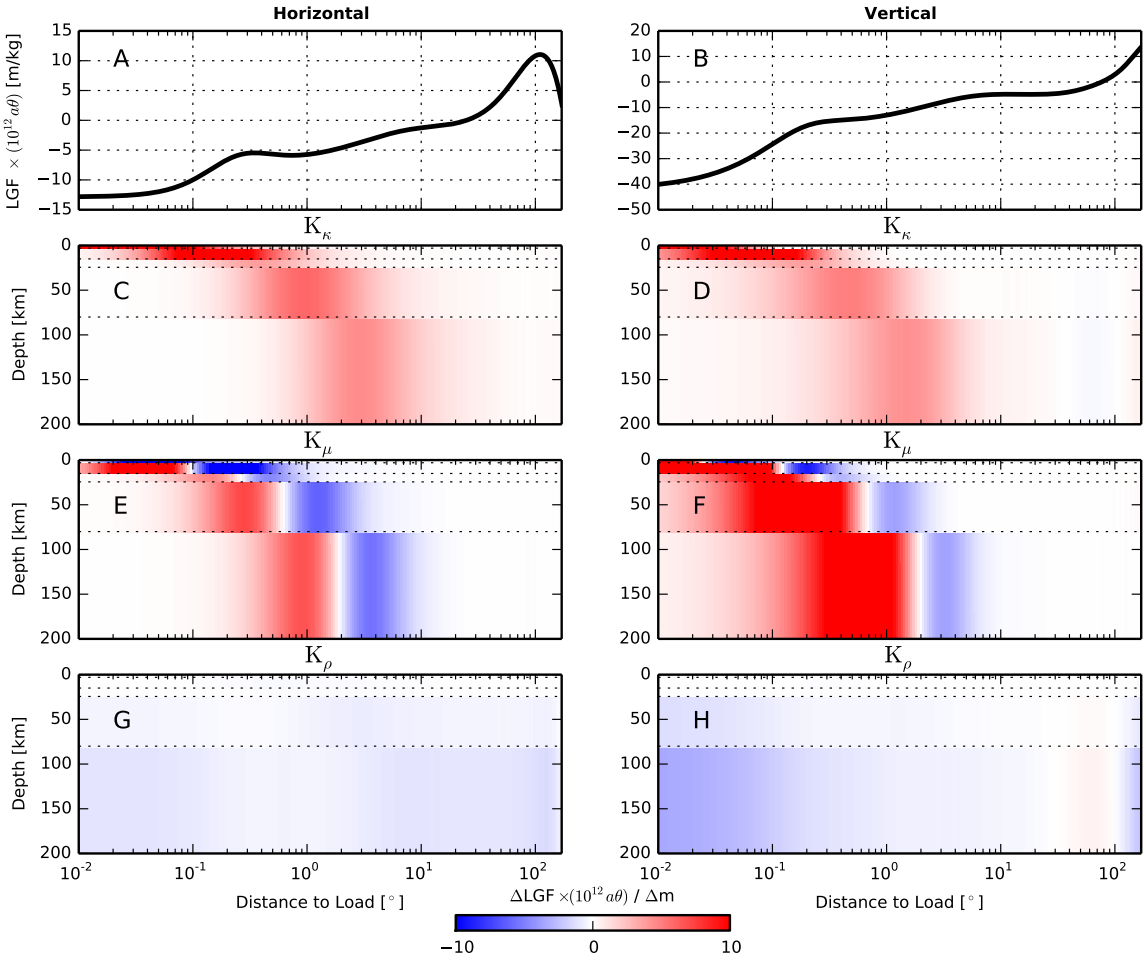

Figure S19. The sensitivity of displacement LGFs to perturbations in elastic structure for a radially heterogeneous Earth model (same as Fig. 6 from the main text, but zoomed into the upper 200 km). We adopted an isotropic and oceanless version of PREM as the reference model. We examine the sensitivity of the displacement LGFs to linear perturbations of 1% to the bulk modulus (panels C and D), shear modulus (panels E and F), and density (panels G and H) as a function of depth. We independently perturb each of the major regions of PREM down to 200 km depth as a distinct blocks, separated by dashed lines in the figure. Model parameters are defined in common-log space as $\mathbf{m}_\mu = \log_{10}\mu$, $\mathbf{m}_\kappa = \log_{10}\kappa$ and $\mathbf{m}_\rho = \log_{10}\rho$. The applied model-parameter perturbation was $\Delta\mathbf{m}_p^j = \log_{10}(1.01)$. The horizontal components of the displacement LGFs and sensitivity kernels are shown in the left panels; the vertical components are shown in the right panels. The top panels (A & B) depict the the displacement LGFs in the CM reference frame derived from the reference model. The displacement LGFs, as well as the sensitivity kernels, were multiplied by the factor $10^{12}a\theta$ to remove the singularity at the load point and to normalize the magnitude of the response, where a is Earth's radius in meters and θ is the angular distance from the load point in radians. Units of the unnormalized LGFs are meters per kilogram.

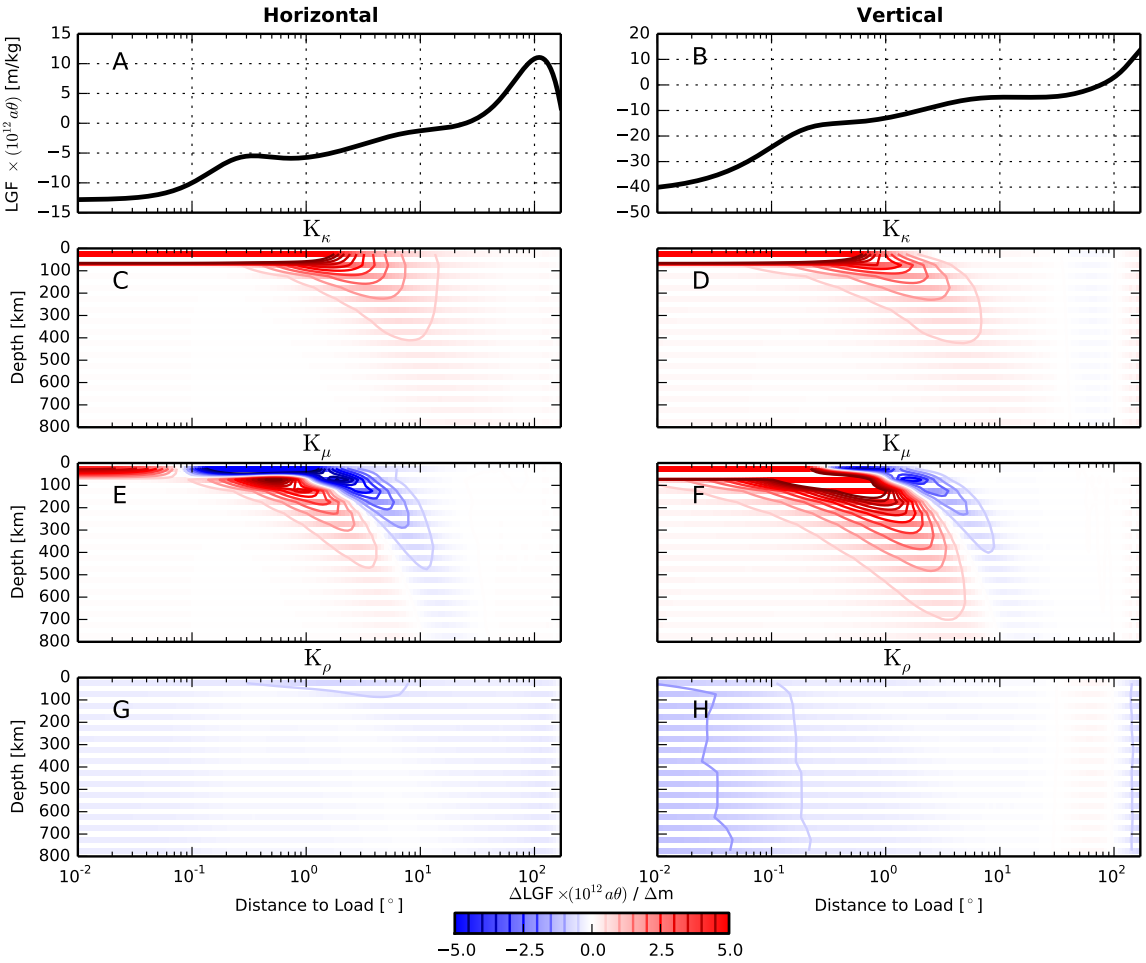

Figure S20. Same as Fig. S19, except that we have perturbed layers of constant thickness instead of the major regions of PREM (cf. Fig. 7 from the main text). Specifically, we have partitioned the crust and mantle into a set of 50-km-thick spherical shells, which we perturb systematically down to 800 km depth. We adopted a model parameter perturbation of $\Delta \mathbf{m}_p^j = \log_{10}(1.01)$. Contour lines are included for clarity, with specific values denoted in the colorbar.

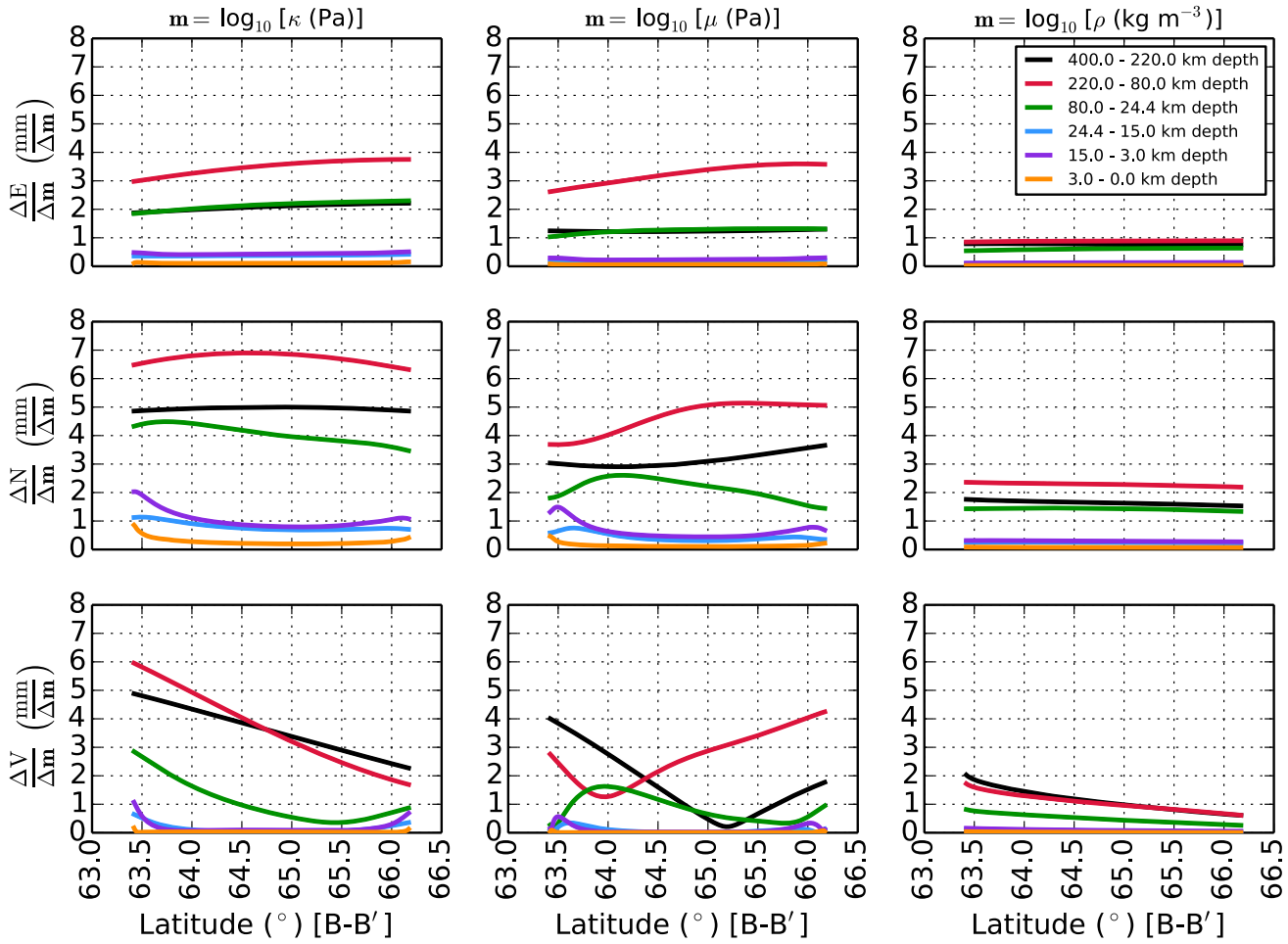

Figure S21. Sensitivities of OTL-induced surface displacements to perturbations in elastic and density structure along a great-circle path through Iceland (profile B–B′ from Fig. 11 in the main text). The profile maintains constant longitude along the 341°E meridian and a node spacing of 0.01° (≈1 km). The left column of panels shows the sensitivity of predicted surface displacements to perturbations in the bulk-modulus model parameter, $\Delta \log_{10} \kappa$. The center column of panels shows the sensitivity to perturbations in the shear-modulus model parameter, $\Delta \log_{10} \mu$. The right column of panels shows the sensitivity to perturbations in the density model parameter, $\Delta \log_{10} \rho$. In each case, we perturb the parameters by 1% in linear space, or by $\Delta \mathbf{m} = \log_{10}(1.01)$ in log space, where $\mathbf{m} = \log_{10} \kappa$, $\log_{10} \mu$, or $\log_{10} \rho$. The top, middle, and bottom rows of panels show sensitivity kernels for OTL-induced surface displacements in the east, north, and vertical components, respectively. The colored lines denote perturbations to distinct layers of PREM down to a depth of 400 km and correspond to the same layer in every panel (see legend). The sensitivity kernels are computed, separately for each layer, as the magnitudes of vector differences between the predicted OTL-induced surface displacements (in millimeters) for the perturbed and reference (unperturbed PREM) models divided by the model-parameter perturbation, $\log_{10}(1.01)$.

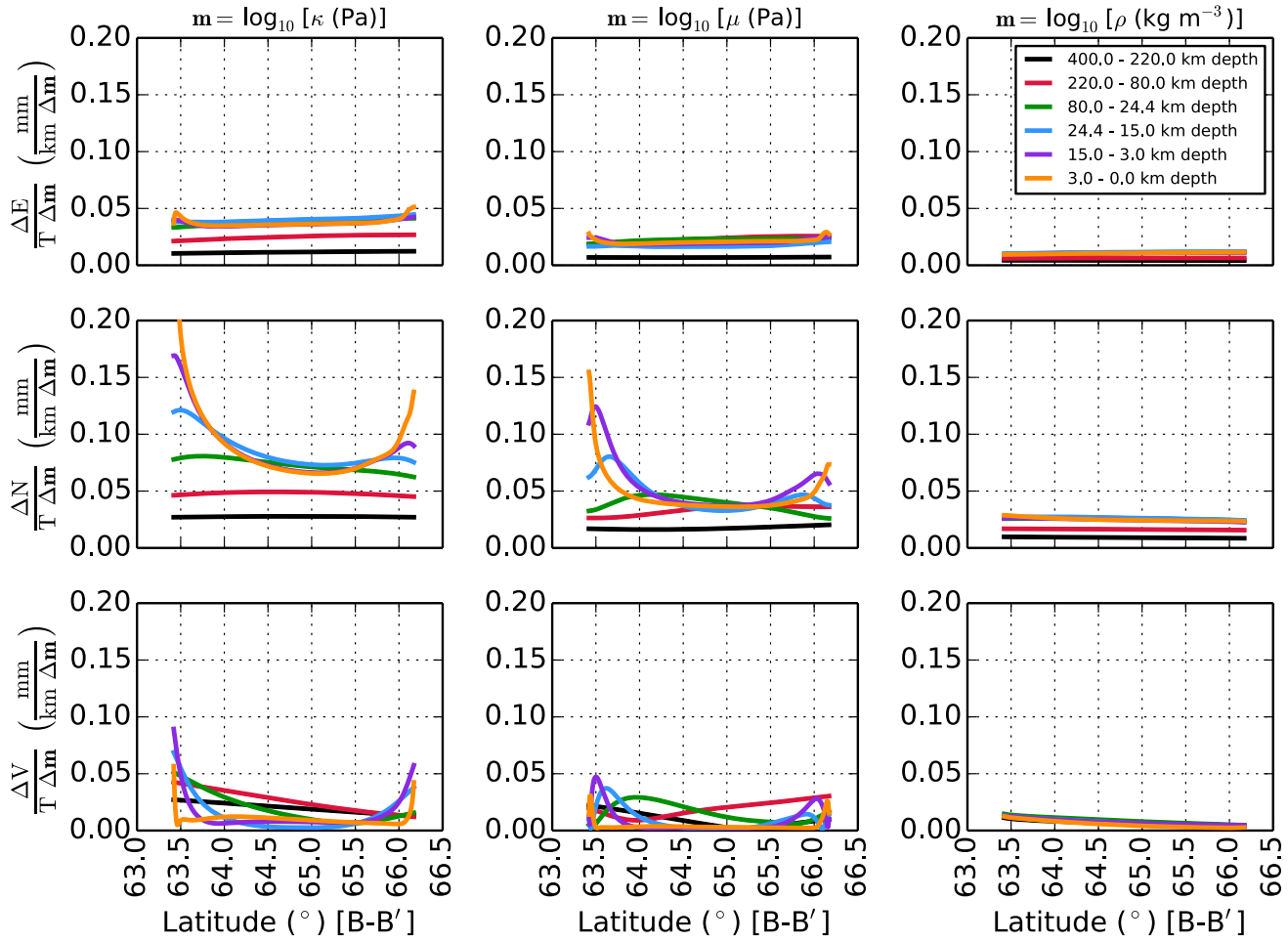

Figure S22. Same as Fig. S21, but normalized by the layer thickness, T (in kilometers).

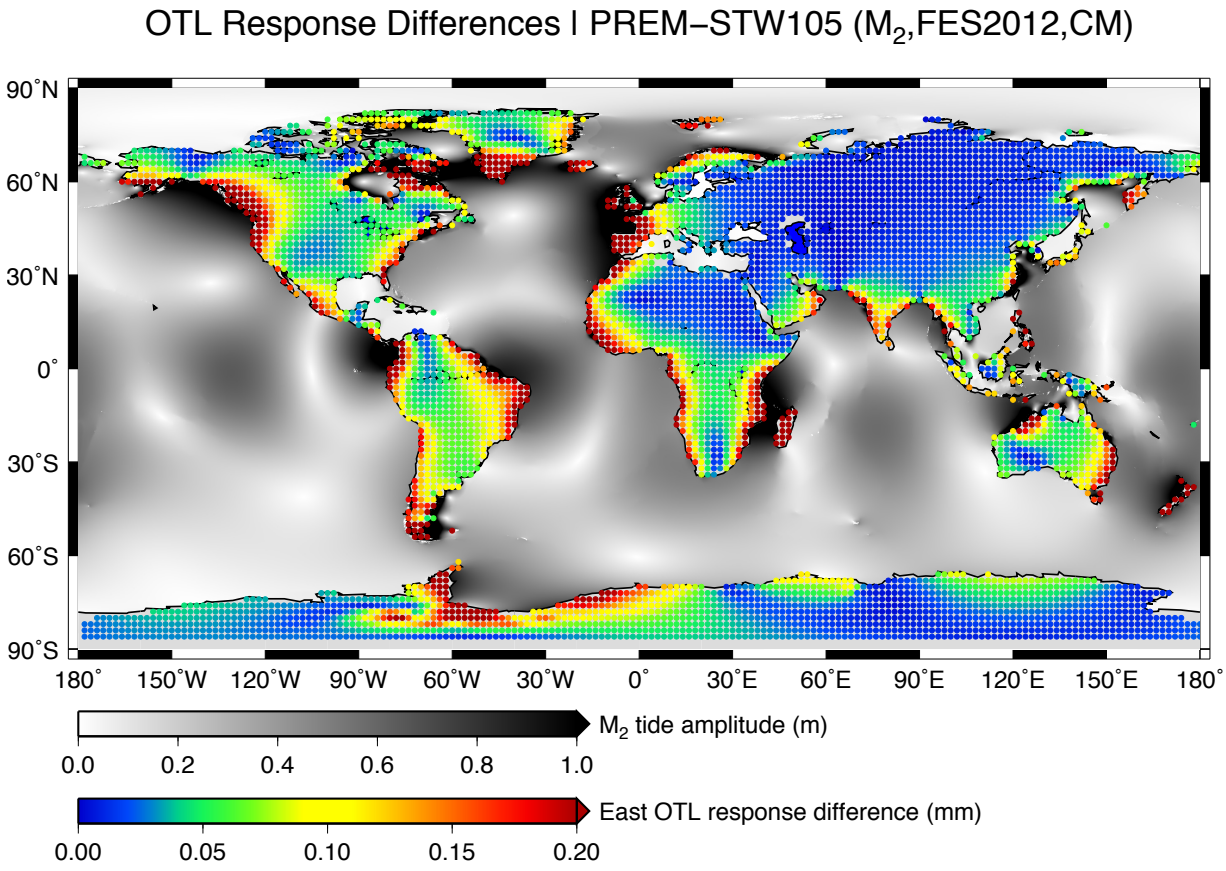

Figure S23. Magnitudes of the vector differences between predicted OTL-induced surface displacements in the east component across a $2^\circ \times 2^\circ$ global grid for two forward models: one computed using LGFs derived from PREM and the other computed using LGFs derived from STW105. All other parameters, including the ocean-tide model and convolution procedure, remain consistent in each forward model computation. Histograms showing the magnitudes of the vector differences between predicted displacements for additional pairs of standard Earth models are shown in Fig. S26.

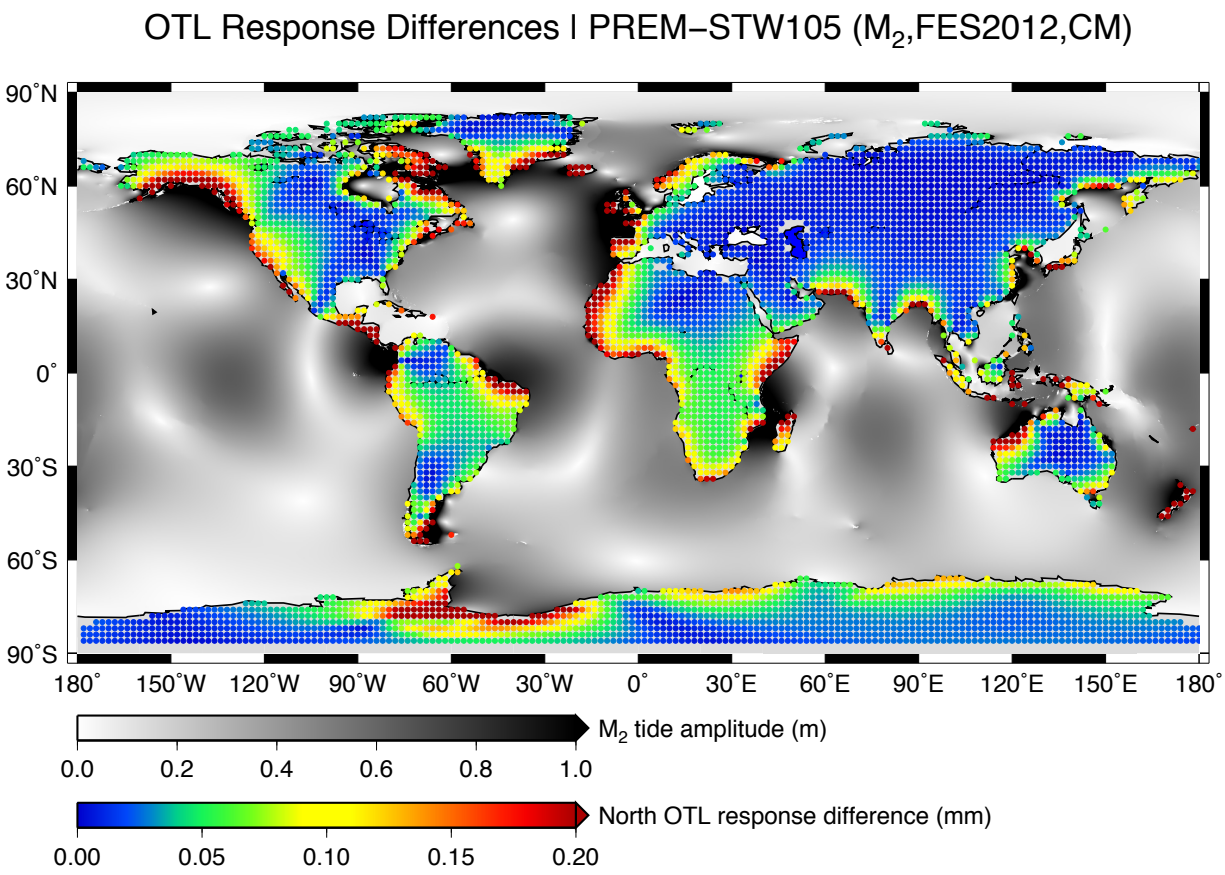

Figure S24. Same as Fig. S23, but for the north component of the predicted displacements.

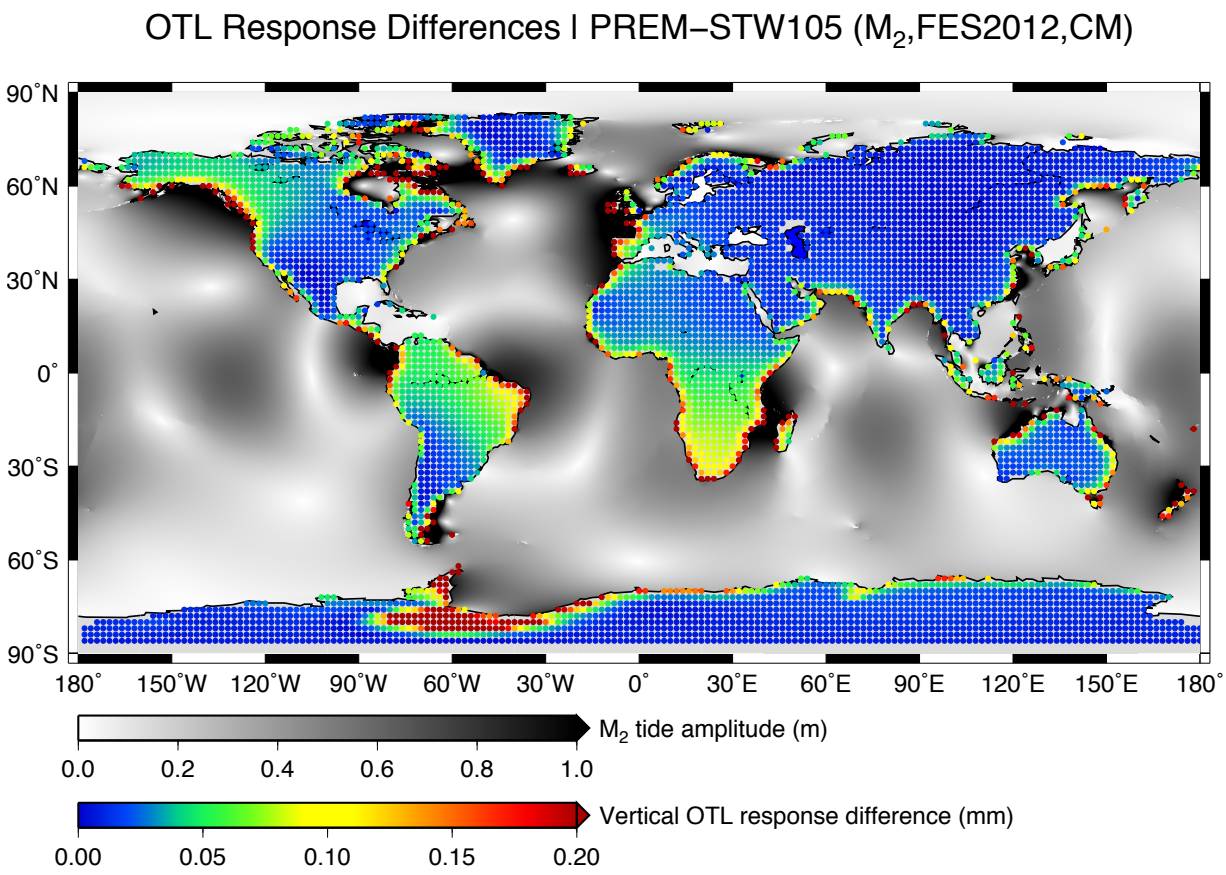

Figure S25. Same as Fig. S23, but for the vertical component of the predicted displacements.

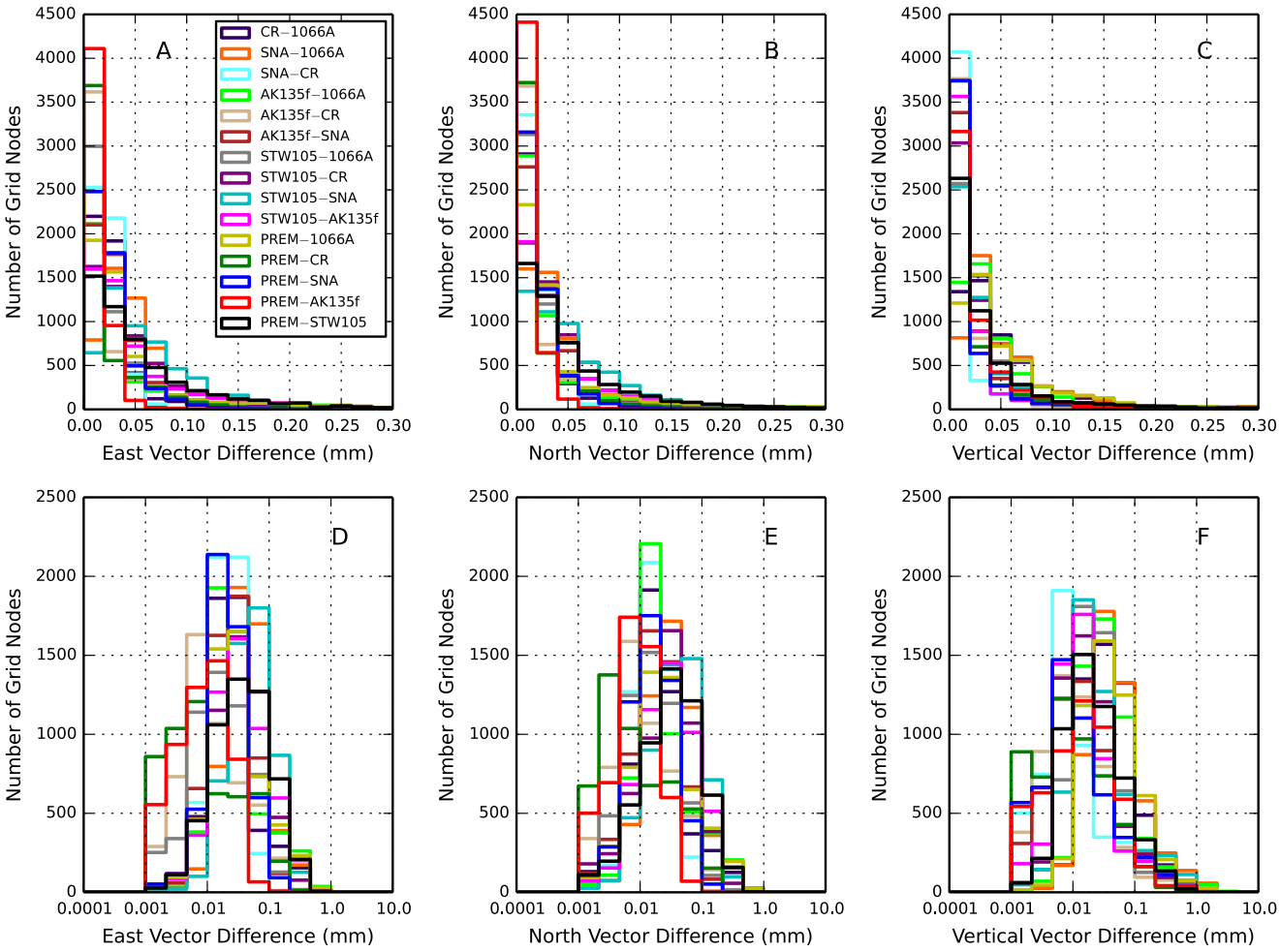

Figure S26. Histograms showing the magnitudes of the vector differences between predicted OTL-induced surface displacements for pairs of reference Earth models. Only the elastic Earth model changes between the forward model computations; all other parameters, including the ocean-tide model and convolution procedure, remain the same. We consider only the M_2 tidal harmonic and predict the response on a $2^\circ \times 2^\circ$ global grid of land-based locations. The left, center, and right panels depict the east, north, and vertical components of the vector differences, respectively. The top row of panels shows the vector differences on a linear scale; the bottom row of panels shows the vector differences on a log scale.

Table S1. Degree-2 potential Love numbers for the seismologically derived SNREI Earth models considered in our study (Data Sets S1–S6).

Model	h_2	l_2
PREM	0.6067	0.0841
STW105	0.6078	0.0839
AK135f	0.6074	0.0847
SNA	0.6069	0.0844
CR	0.6054	0.0837
1066A	0.6130	0.0851